DOKUZ EYLÜL UNIVERSITY
GRADUATE SCHOOL OF NATURAL AND APPLIED SCIENCES

RADAR PULSE REPETITION INTERVAL RECOGNITION AND REAL-TIME DETECTION UNDER NON-GAUSSIAN NOISE

by
Bora COŞKUN

September, 2019
İZMİR

RADAR PULSE REPETITION INTERVAL RECOGNITION AND REAL-TIME DETECTION UNDER NON-GAUSSIAN NOISE

A Thesis Submitted to the
Graduate School of Natural and Applied Sciences of Dokuz Eylul University
In Partial Fulfillment of the Requirements for the Degree of Master of Science in Electrical and Electronics Engineering

by
Bora COŞKUN

September, 2019
İZMİR

M.Sc THESIS EXAMINATION RESULT FORM

We have read the thesis entitled **"RADAR PULSE REPETITION INTERVAL RECOGNITION AND REAL-TIME DETECTION UNDER NON-GAUSSIAN NOISE"** completed by **BORA COŞKUN** under supervision of **ASSIST. PROF. DR. MEHMET EMRE ÇEK** and we certify that in our opinion it is fully adequate, in scope and in quality, as a thesis for the degree of Master of Science.

Assist. Prof. Dr. Mehmet Emre ÇEK

Supervisor

Doç. Dr. M. Alper Selver

(Jury Member)

Prof. Dr. Mustafa SEÇMEN

(Jury Member)

Prof.Dr. Kadriye ERTEKİN

Director
Graduate School of Natural and Applied Sciences

ACKNOWLEDGEMENT

I would first like to thank my thesis advisor Assist. Prof. Dr. Mehmet Emre ÇEK of the Graduate School of Natural and Applied Sciences at Dokuz Eylul University. The door to Assist. Prof. ÇEK office was always open whenever I ran into a trouble spot or had a question about my research or writing. He consistently allowed this paper to be my own work, but steered me in the right the direction whenever he thought I needed it.

I would also like to acknowledge Assist. Prof. Dr. Ozan Sabahattin SARIYER of the Faculty of Arts and Sciences at Piri Reis University and I am gratefully indebted to his for his very valuable comments on this thesis.

Finally, I'd like to thank my wife, Zeynep, and my daughter, Asya, who put up with my long hours seeing this thesis to completion.

Bora COŞKUN

RADAR PULSE REPETITION INTERVAL RECOGNITION AND REAL-TIME DETECTION UNDER NON-GAUSSIAN NOISE

ABSTRACT

In this thesis study, feature extraction related with Pulse Repetition Interval (PRI) modulation recognition, as one of the essential processes in Electronic Support (ES) receivers, and the detection of PRI modulated signals under non-Gaussian noise is investigated. The discriminative feature extraction methods in the thesis are primarily based on autocorrelation and power spectral density similar to the literature. The main contribution is the recovery of rectangular pulse onset under $\boldsymbol{\alpha}-$Stable noise environment which exhibits impulsive non-Gaussian behavior.

The first proposed approach is to utilize robust estimators which give limited time of arrival estimation performance depending on the impulsiveness of the channel noise and used robust filter length. As another novel contribution, time-varying cumulative summation (CUSUM) based quickest detection (QD) method is adapted to detect pulse onset with minimum time delay. It is shown that raw PRI modulated waveforms under non-Gaussian noise can be tracked to detect rising edge of the rectangular radar pulses with minimum time delay depending on the selection of proper threshold which is directly related with probability of false alarm.

Keywords: Electronic Support (ES), pulse repetition interval (PRI) modulation, autocorrelation, power spectral density, robust estimators, quickest detection method, time varying CUSUM algorithm

DARBE TEKRARLAMA ARALIĞI TANIMASI VE GAUSS OLMAYAN GÜRÜLTÜ ALTINDA GERÇEK ZAMANLI TESPITI

ÖZ

Bu tez çalışmasında, Elektronik Destek (ED) alıcıları için önemli bir işlem olan Darbe Tekrarlama Aralığını (DTA) tanımlama ve Gaussyen olmayan gürültü altında gerçek zamanlı tespit edilmesi incelenmiştir. Tezdeki ayırt edici karakteristik çıkarım yöntemleri, literatürdekine benzer biçimde, özelikle özilinti ve güç spektrum yoğunluğu tabanındadır. Tezin ana katkısı, Gaussyen olmayan dürtüsel davranış gösteren α-kararlı gürültü ortamındaki dikdörtgen biçimli darbe eşiğinin geri kazanılmasıdır.

Önerilen ilk yaklaşım, kanal gürültüsünün dürtüselliğine ve kullanılan gürbüz filtre uzunluğuna bağlı olarak kısıtlı bir varış zamanının tahminine ilişkin performansını veren, gürbüz kestiricilerden istifade etmektir. Bir başka yeni katkı olarak, minimum zaman gecikmeli darbe eşiği algılanması için zamanla değişen kümülatif toplam (CUSUM) tabanlı en hızlı algılama (QD) yöntemi uyarlanmıştır. Yanlış alarm olasılığıyla doğrudan ilişkili uygun eşik seçimine bağlı olarak minimum zaman gecikmesiyle dikdörtgen biçimli radar darbelerinin yükselme köşesinin algılanmasında, Gaussyen olmayan gürültü altındaki ham DTA kipleminin dalga formlarının izlenebileceği gösterilmiştir.

Anahtar Kelimeler: Elektronik Destek (ED), Darbe Tekrarlama Aralığı (DTA) kiplenimi, özilinti, güç spektrum yoğunluğu, gürbüz kestiriciler, en hızlı algılama (QD) yöntemi, zamanla değişen CUSUM algoritması

LIST OF FIGURES

Page

LIST OF TABLES

Page

CONTENTS

Page

CHAPTER ONE
INTRODUCTION

1.1 Electronic Warfare (EW) and Chronicle

Sun Tzu highlighted the importance of intelligence regarding the battlefield as follows: “If you know the enemy and know yourself, you need not fear the result of a hundred battles. If you know yourself but not the enemy, for every victory gained you will also suffer a defeat. If you know neither the enemy nor yourself, you will succumb in every battle.” (Giles, 1910). History repeatedly has demonstrated that an armed force can win against an opposition of superior quality and quantity, if they make use of accurate intelligence. Successful duty of modern weapons systems and innovative combat techniques depend on swift, definite, accurate, and detailed intelligence.

Today's modern armed force structure is based on the technological superiority of electronic systems rather than quantitative superiority. The electromagnetic environment appears extensively in all operation areas, while the usage of the electromagnetic spectrum is advanced due to technological developments and therefore the precision of the systems and equipment’s in the electronic warfare (EW) is increased.

In today’s battles, the initiative is on the side of the EW supremacy, and such supremacy will play even more important roles in winning military victories in the near future. With the developments in signal processing technology, intelligent algorithms will start to be used in weapon systems and it will be difficult for electronic attack activities such as deception. In this context, reverse engineering activities will gain importance in solving algorithms for protection against weapon systems, and for quick detection and identification of enemy elements.

First and most important phase of the war is to make the distinction thoroughly between friendly, hostile and neutral elements. Thanks to proper identification in the operational area, neutral elements can be prevented from attacking, the forces can be

protected from friendly fire, and enemy elements can be actively engaged. The identification process is carried out on the basis of the position determination, recognition and classification stages. The intelligence obtained from the enemy elements makes an important contribution to the identification process. In this context, it is possible to classify enemy radar emitters on the basis of Nationality, Platform, Type, Class and Unit by analysing electronic intelligence (ELINT) obtained through sensors.

One might count the U.S. Civil War in 1861 as the beginning of the history of EW. In the historical journey of telegraph – invented by Samuel Morse in 1837 – an important step was recorded with the establishment of the transatlantic telegraph line in 1858. When American Civil War began in 1861, telegraph wires became one of the most important targets for infantry and especially cavalry. Cavalry men changed military telegraph traffic to the inaccurate destinations deliberately, and transmitted false orders to Union commanders. These can be thought of as early applications of modern "intelligence" activities in the military concept of "command, control, communications, and intelligence". Although telegraph technology is not considered a part of the EW because it does not radiate electromagnetic energy, these tactics are the first examples of signal intelligence, jamming and deception. Table 1.1 shows the conspicuous case till end of the WWI, including technological developments that led the way for EW.

Table 1.1 Conspicuous case till end of the WWI

Date	Event
1837	S. F. B. Morse invents telegraph.
1858	The transatlantic undersea cable for communication is established between U.S. and Britain.
1861	During the U.S. Civil War, the telegraph lines becomes an important target for enemy cavalry.
1865	J. C. Maxwell proved theoretically the existence of the electromagnetic field.
Early 1870s	J. C. Maxwell's theory established the basis of propagation of electromagnetic waves in free space.
1888	H. Hertz demonstrated the existence of the electromagnetic waves.
1895	Captain H. Jackson's radio system transmits Morse signal over 100 yards in England.
1897	G. Marconi sent and received signals over two miles.
1899	G. Marconi radio sequences improvement the transmission range to 89 miles.
1901	The first recorded example of intentional radio jamming in the U.S.
1902	British Navy Fleet exercises in the Mediterranean.
1903	U.S. Navy Fleet uses jamming.
1904-1905	Radio jamming is used in a war for the first time to obtain tactical advantage during the Russian-Japanese War.
1906	The U.S. Navy installed a direction finder on the coal ship Lebanon for trial purpose.
1915	Royal Navy began establishing direction finder stations around the east coast of England.

EW, for the purpose of attack or impede enemy attack, is every deliberate activity including the use of the electromagnetic spectrum and directed energy. The three major subdivisions within EW are electronic attack, electronic protection and electronic support. Figure 1.1 shows the classification of EW.

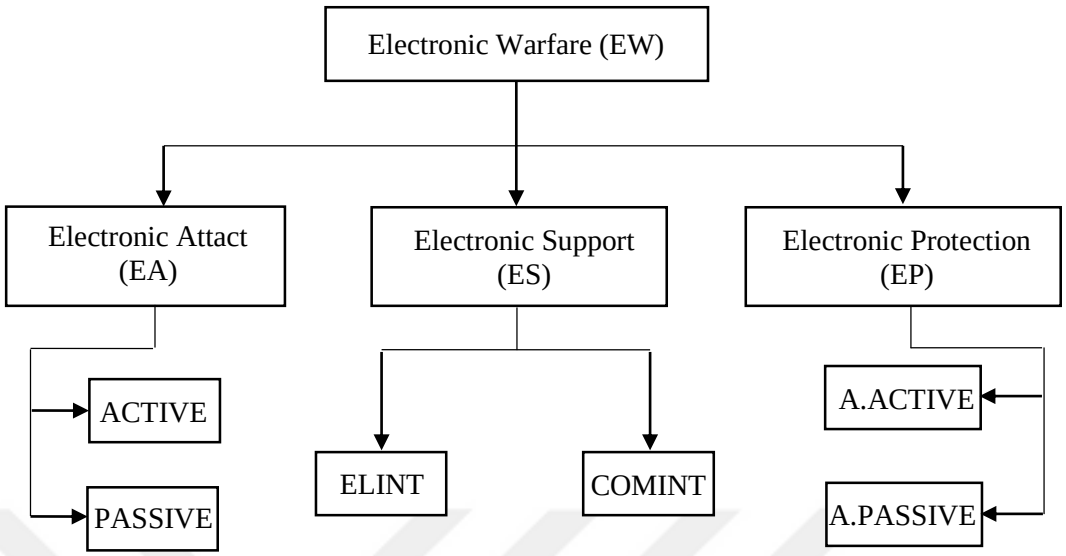

Figure 1.1 EW Classification (Poise, 2013)

1.1.1 Electronic Attack

Electromagnetic or directed energy can be used to attack enemy facilities, equipment or personnel, in order to degrade, neutralize or destroy their ability to use electromagnetic spectrum. Examples of Electronic Attack (EA) are the usage of jamming systems and anti-radiation weapons. EA consists of the following actions:

- All actions to impede or degrade an enemy's effective use of the electromagnetic spectrum, such as jamming and electromagnetic deception.

- Usage of electromagnetic energy as destructive contraption, such as lasers, radio frequency weapons, etc. (Poise, 2013).

1.1.2 Electronic Protection

Electronic Protection (EP) includes all active and passive actions taken to protect personnel, facilities and equipment from enemy attacks that can impede, neutralize or

destroy. Examples include Emission Control (EMCON) plan, filtering out harmful wavelengths of laser, EW reprogramming, and frequency switching (Poise, 2013).

1.1.3 Electronic Support

Electronic Support (ES) includes all actions to search for, intercept, locate, record, identify and analyze enemy usage of the electromagnetic spectrum. The primary purpose of ES during these activities is the threat recognition, prioritization and taking precaution. These activities can also be used to produce Signal Intelligence (SIGINT). SIGINT consists of Communications Intelligence (COMINT) and Electronic Intelligence (ELINT), where COMINT activities supply intelligence derived from intercept of enemy communications. Radio teletype, Morse code, facsimile, multi-channel, and video signals can be analysed with COMINT. The subject of this thesis is within the scope of the second subtype of ES, namely the ELINT, which is the identification and classification of the enemy's communications electronic systems and radar sensors. Such activities play an important advantage for friendly associations in the field of operations (Poise, 2013).

Information can be gathered from electromagnetic transmitter systems such as weapon systems, radars and other sensors. This is achieved for the purpose of extracting information of some intelligence value, by the detection and analysis of radiations from enemy electronic devices.

ELINT is the analysis of the incoming signals from threat radars, including surveillance, targeting and missile guidance systems. Signals from radar systems are intercepted by a warning receiver and are analyzed by a joint processor to give frequency (fr), pulse width (PW), pulse repetition interval (PRI), scan pattern, scan type, angle of arrival (AoA), and amplitude (A), as shown in Figure 1.2 below (Gençol & Kara, 2016; Liu & Zhang, 2017; Ghani et al. 2017). These parameters are generally sufficient to characterize the type of emitter. The recognition is then carried out by comparing the analyzed signal with parameters of hostile, friendly and neutral emitter characteristics stored in a library within the computer memory. Analysis of the

signals and warning of a threat must actually be abrupt, since there can be countermeasures of jamming and/or decoys that can be initiated swiftly by the enemy.

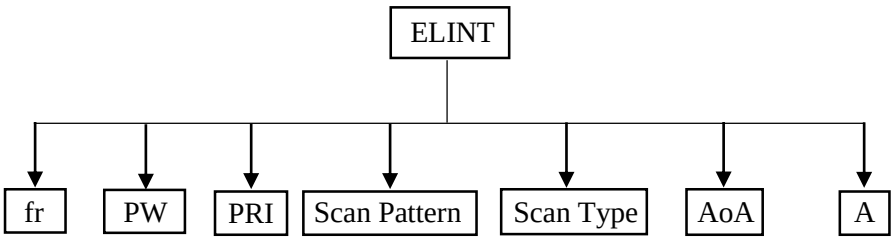

Figure 1.2 Parameters of an incoming signal obtained by an ELINT system

1.2 Radar Frequency Interval within Electromagnetic Spectrum

In this section, it is more convenient to provide a brief note on the electromagnetic spectrum, for its application in EW systems is the main theme of this thesis. Electromagnetic spectrum is a regular distribution of electromagnetic waves according to their frequency (or wavelength), as depicted in Figure 1.3 The spectrum is divided into bands ranging from radio frequencies at the low end to X-ray and gamma frequencies at the high end.

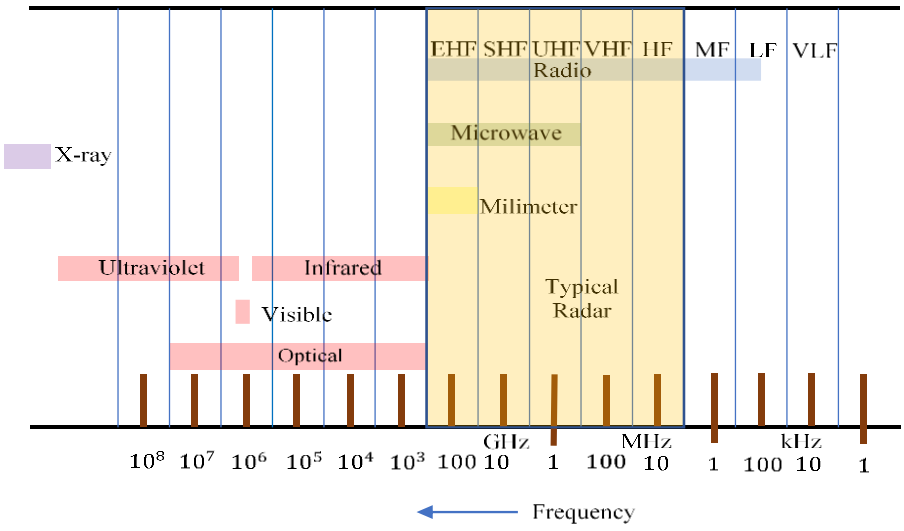

Figure 1.3 Graphical depiction of the electromagnetic spectrum (Avionics Department, 2013; Joint Chiefs of Staff, 2012; Skolnik, 1981)

The electromagnetic spectrum contains the following bands in increasing frequency (or decreasing wavelength):

- Radio waves,
- Micro waves,
- Visible light,
- X rays,
- Electromagnetic cosmic rays and gamma rays.

Depending on the operation purpose, radars operate within the frequency range of 3 Mhz to 300 Ghz of the electromagnetic spectrum (Skolnik, 1981; Skolnik, 1990). Surveillance radars operate at low frequencies, search radars at intermediate frequencies, and tracking radars at high frequencies (see Table 1.2). When the frequency value of the radar with a fixed output power is increased, the coating range is reduced. But after all, the trailing quality within the coating range increases with increasing frequency. It is estimated that radar frequencies can be increased to 60-90 GHz in the mid-range, to 300 GHz in the long-term, but the atmosphere will continue to be a major limiting factor at these high frequencies.

Table 1.2 Operational frequency bands for different radars (Skolnik, 1990)

Band	Frequency	Usage
HF	3-30 MHz	HF Radars
VHF	300-1000 MHz	VHF Radars
UHF	300-1000 MHz	Airborne Early Warning Radars
L	1-2 GHz	Land-Based Long-Range Air Surveillance Radars
S	2-4 GHz	Long-Range Airborne Surveillance Radars
C	4-8 GHz	Multifunction Phased Array Air Defense Radars Medium-Range Weather Radars
X	8-12 GHz	Doppler Navigation Radars Weather Avoidance Radars Shipboard Navigation and Piloting Radars Weapon Control (Tracking) Radars Police Speed Meter Radars
Ku	12-18 GHz	Airport Surface Detection Radars Ground Traffic at Airports Radars
K	18-26.5 GHz	Little Use (Water Vapor)
Kn	26.5-40 GHz	Very High Resolution Mapping Airport Surveillance
Milimeter	40-100+ GHz	Experimental

CHAPTER TWO
MEASUREMENT AND ANALYSIS OF PRI PATTERNS

As a general procedure, when signals are detected by ES systems, they are first deinterleaved and clustered, and then identified. During the deinterleaving and clustering step, incoming pulses are separated from the detected wave and associated with separate sources. Therefore, before the identification process, incoming waves have to be deinterleaved into distinct sources.

2.1 De-Interleaving

Deinterleaving the pulse trains has been studied by many researches in the past decades (Moore & Krishnamurthy, 1994; Conroy & Moore, 1998; Orsi, Moore & Mahony, 1999; Conroy & Moore, 2000; Davies & Hollands, 1982; Mardia, 1989; Milojevic & Popovic; 1992). In a conventional modern operation area, typically several complex PRI modulation types should be expected, and these PRI modulation types may overlap. Therefore, deinterleaving has been an important aspect for the recognition of a single PRI modulation for the detailed analysis. It is done by signal sorting to separate each pulse from a signal flow of a large number of overlapping pulses – some of which are random noise or jam – and then selecting the useful "**deinterleaved**" signals. Several pulse characteristics including pulse width (PW), radio frequency (RF), angle of arrival (AoA), and the inter-pulse time of arrival (TOA) are clustered for a successful deinterleaving procedure. Figure 2.1 shows the typical scheme of deinterleaving process.

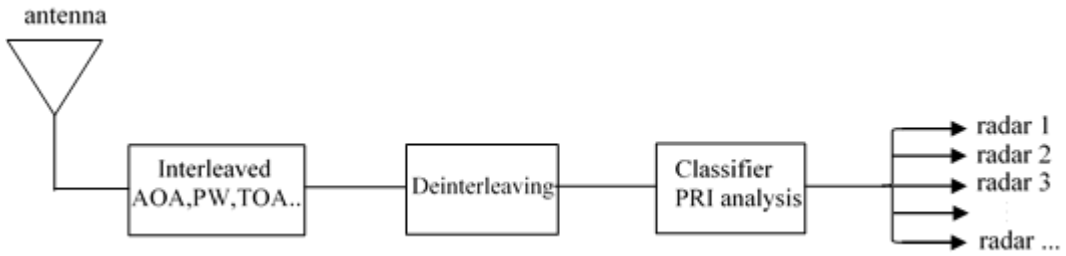

Figure 2.1 Typical deinterleaving process scheme. Overlapping (interleaved) signals are received by an antenna. The deinterleaving process separates different signals and classifies them according to signal parameters such as AoA, PW, ToA, *etc*.

In the literature, it is also a common approach to concentrate on de-interleaved signals or signals which are not interleaved, for PRI characterization. For this purpose, CDIF and SDIF methods are assumed to be useful in extracting constant PRI and staggered PRI modulations during pulse deinterleaving procedure (Mardia, 1989; Kuang & Shi, 2005; Ghani et al. 2017).

2.2 Radar Parameters

Signal recognition allows the selection and extraction of properties of known signal transducer properties. Data from the classifier sequentially compares specific signal parameters with those in a library to determine possible identities of the received signals. The radar parameters directly measurable by the Electronic Intelligence (ELINT) systems are as follows (Avionics Department, 2013; Kumar & Dhananjayulu & Kumar, 2014):

- Radio (Carrier) Frequency (RF),
- Pulse Width (PW),
- Scan Pattern,
- Angle of Arrival (AoA),
- Signal Amplitude (A),
- Polarization,
- Time of Arrival,
- Pulse Repetition Interval (PRI).

All parameters except PRI can be shortly described as follows:

i) Radio (Carrier) Frequency (RF)

Most radars are designed with frequency agility to make detection and identification difficult. This change in the frequency may be at random times or at a specific period of time, such as pulse to pulse or group to group period.

ii) Pulse Width (PW)

PW of a radar determines its resolution. Radars infrequently switch their PW for not to be detected. The PW measurement precision is related to pulse amplitude. For small pulse amplitude, the PW measurement may be incorrect even for high signal-to-noise-ratio (SNR).

iii) Scan Pattern

Scan pattern is how radars direct their beam across their field of view to search for targets. General scan patterns are:

- Circular scan,
- Linear scan,
- Conical scan.

iv) Angle of Arrival (AoA)

AoA is determined by the elevation and azimuth angle of received signals, and it is also called the direction of arrival (DoA).

v) Pulse Amplitude (A)

The amplitude of the rectangular pulse is directly related with the detection capability of the individual pulse and/or group of pulses under certain signal to noise ration. This parameter is tuned to provide prescribed signal to noise ratio requirement.

vi) Polarization

Polarization is the oscillations that indicate the geometric direction of the waves of radars and move along a sequence. It can be used as a parameter for identification.

vii) Time of Arrival (ToA)

Time of arrival (ToA), is considered to be the receiving time of a rectangular radar pulse from a single transmitter to a remote single receiver. The measurable arrival time of the radars is directly related to the PRI parameter. For this purpose, PRI values can be changed in different types. Radars can change PRI modulations to prevent the identification or to improve ES capabilities.

The ToA of a signal pulse is, as the name suggests, the instant that the pulse is received. It might be taken as the time when the received amplitude exceeds a predetermined threshold. Although such a measurement of ToA is threshold-dependent and not super-precise in the presence of noise and distortion, it can still be used for the determination of PRI up to an accuracy (Skolnik, 1990).

2.3 Pulse Repetition Interval (PRI)

PRI modulation can be used in the base processes by ES receivers for the purpose of recognition. The recognized PRI modulation type usually reveals the emitter identification and classification, and it can be used to determine the functional purpose of the radar.

PRI is the time required for a radar's complete transmission cycle. Alternatively, it can be described as the time interval from the commencement of a pulse of energy to the beginning of the next pulse, shown in Figure 2.2. The unit of PRI sequence is assessed as microseconds.

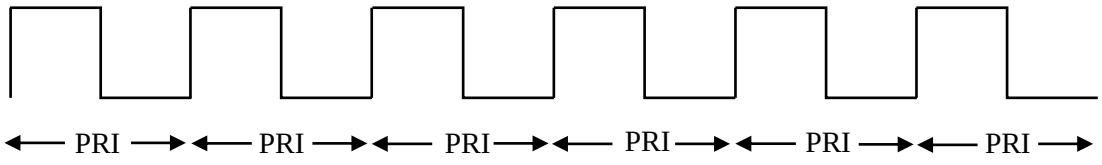

Figure 2.2 A pulse train in time domain. PRI is the time between consecutive pulses

In general, PRI of the nth pulse X_n can be defined as the function of ToA as represented by (2.2)

$$X_n = t_{n+1} - t_n \qquad n = 1,2,\ldots..,N-1 \tag{2.1}$$

where t_n is the ToA of the nth pulse received in a pulse sequence having length of N samples, and X_n is the difference of ToAs of two consecutive pulses, *i.e.*, nth and $(n+1)$th. (Mahdavi & Pezeshk, 2010).

Noting that PRI is determined by the interval between adjacent pulses, it constitutes a distinctive signature o identify the PRI modulation type. In recent radar production technologies, many types of PRI modulations are used. The most common PRI modulation types are (Wiley, 2006, Logothetis & Krishnamurthy, 1998, Liu & Zhang, 2017):

- Constant,
- Jittered,
- Staggered,
- Sliding,
- Wobulated,
- Dwell & switch.

Since different modulation types are used for distinct purposes, they some significant properties of their emitters. Information on the PRI modulation of a radar signal plays an important role in defining the radar signal in terms of the effective use of the ES system. Once the PRI modulation type is recognized, the information related with type of the target can be achieved.

Emitters with monopulse parameters can be measured using a single pulse. All parameters can be detected on a pulse-by-pulse basis by receivers. Carrier frequency is a proper parameter for emitter recognition, since most radars operate at a single frequency. One can obviously consider pulse width as another parameter for emitter

recognition. However, in practice, it is sensitive to distortions due to effects of reflections. Therefore, identifier effect of pulse width itself is considered to be limited. ES systems use both frequency and AoA features to separate the incoming adjacent pulses from the previously received ones. Amplitude cannot be directly used for emitter recognition but it can be used for classification and for distance evaluation using compiled emitter energy. Furthermore, amplitude and ToA can be used to determine the emitter's scan characteristics. The potential utilization of radar parameters are justified in Table 2.1 according to the deinterleaving and identification performance (Avionics Department, 2013).

Table 2.1 Functionality of emitter parameters in radar signal processing (Avionics Department, 2013)

Parameter	**De-Interleavement**	**Emitter Identification**
Frequency	Proper	Proper
Amplitude	Limited	Improper
AoA	Proper	Improper
ToA	Improper	Improper
PW	Proper	Improper
Scan Pattern	Improper	Improper
PRI	Proper	Proper

In the following subsections, it is concentrated on the definitions and mathematical expressions characterizing different PRI modulation types and illustrated the different PRI modulations derived from exact rectangular pulse train signal generated at MATLAB environment.

2.3.1 Constant PRI Modulation

In this type of PRI modulation, time interval between each consecutive pulse is constant, or variations are typically less than 1% of the average PRI value. The constant PRI exhibiting strongly stable behaviour is generally used in moving target indicator in pulse Doppler radar systems (Wiley, 2006). Typically, the nth PRI value X_n^{co} in constant PRI modulation, is assigned to a constant value r in the order of μsec and formulated as in (2.2):

$$X_n^{\mathrm{co}} = r \qquad n = 1,2,3,\dots,N. \tag{2.2}$$

where N is number of pulses in the observed data and the value of r lies in the specified range in terms of samples for each independent realization. In Figure 2.3a and 2.3b, the pulse train signals with noise and without noise are shown, respectively.

a)

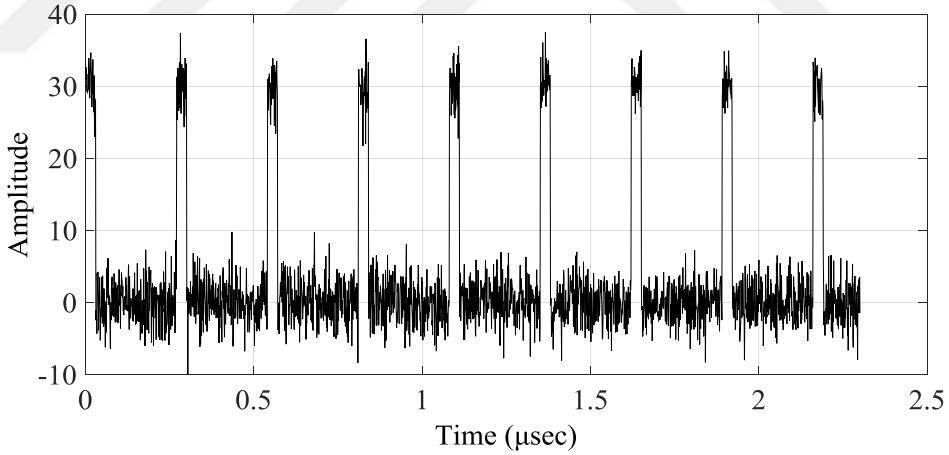

Figure 2.3 Constant PRI modulation signal a) with Gaussian noise $SNR = 18\ dB$ b) Noise free

b)

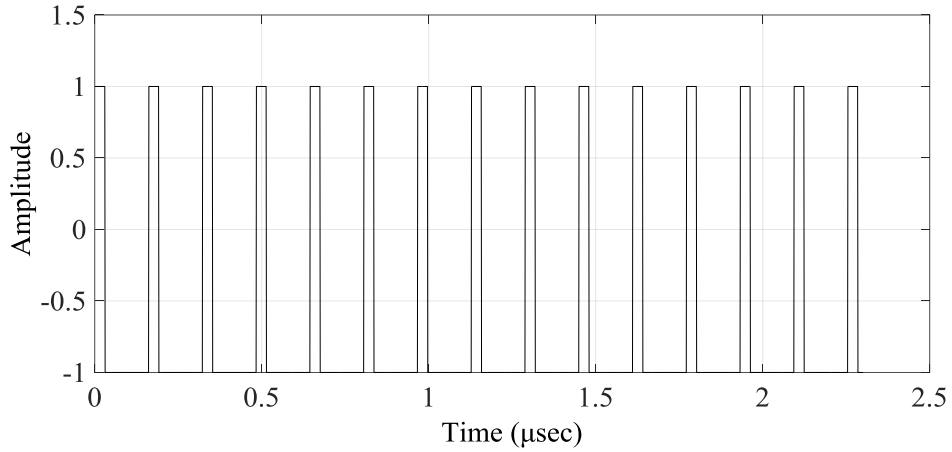

Figure 2.3 continues

2.3.2 Jittered PRI Modulation

In jittered mode, the time interval between successive pulses is allowed to vary randomly among predetermined minimum and maximum values. In a common jittered mode, the PRI sequence X_n^{jit} oscillates up to 30% of the average PRI and is represented by (2.3) (Noone, 1999).

$$X_n^{jit} = \lfloor r_n \rfloor \qquad n = 1,2,3,\dots,N \tag{2.3}$$

where $\lfloor r_n \rfloor$ is rounded integer values of random variable r_n taken from specified probability density function (pdf). Conventionally, the pdf is assumed to be Gaussian shown as (μ, σ^2) . Typically, the mean value μ and standard deviation σ ranges of $\lfloor \mu/10 \rfloor \leq \sigma \leq \lfloor \mu/2 \rfloor$, respectively. As an illustrative example, the pulse train in the time domain with and without noise associated with jittered PRI are given in figure 2.4.

a)

b)

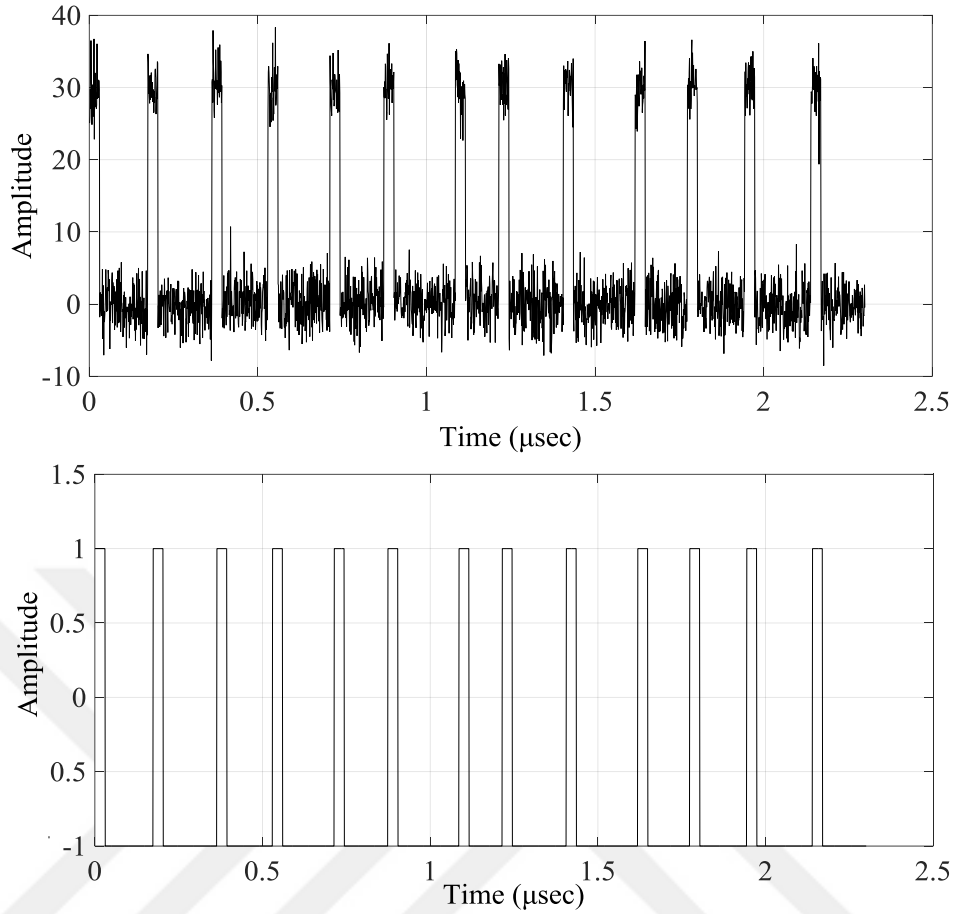

Figure 2.4 Jittered PRI modulation signal a) with Gaussian noise $SNR = 18\ dB$ b) Noise free

2.3.3 Staggered PRI Modulation

In staggered PRI modulation, a fixed random PRI sequence of is repeated periodically along with generated pulse train (Wiley, 2006). Typically, length k of the fixed sequence has the range of $3 \leq k \leq 10$ samples for each realization. The fixed sequence that is repeated is expressed as (2.4)

$$B_i = r_i \qquad i = 1,2,\dots,k \tag{2.4}$$

where r_i is randomly chosen in the range $50\ \mu sec$ to $500\ \mu sec$. The PRI sequence of length N is then constructed from the base set and formulated by (2.5)

$$X_n^{\mathrm{st}} = B_{1+\mathrm{mod}_k(n-1)} \qquad n = 1,2,3,\dots,N \tag{2.5}$$

In Figure 2.5, it is presented a simulated staggered PRI modulation with and without noise.

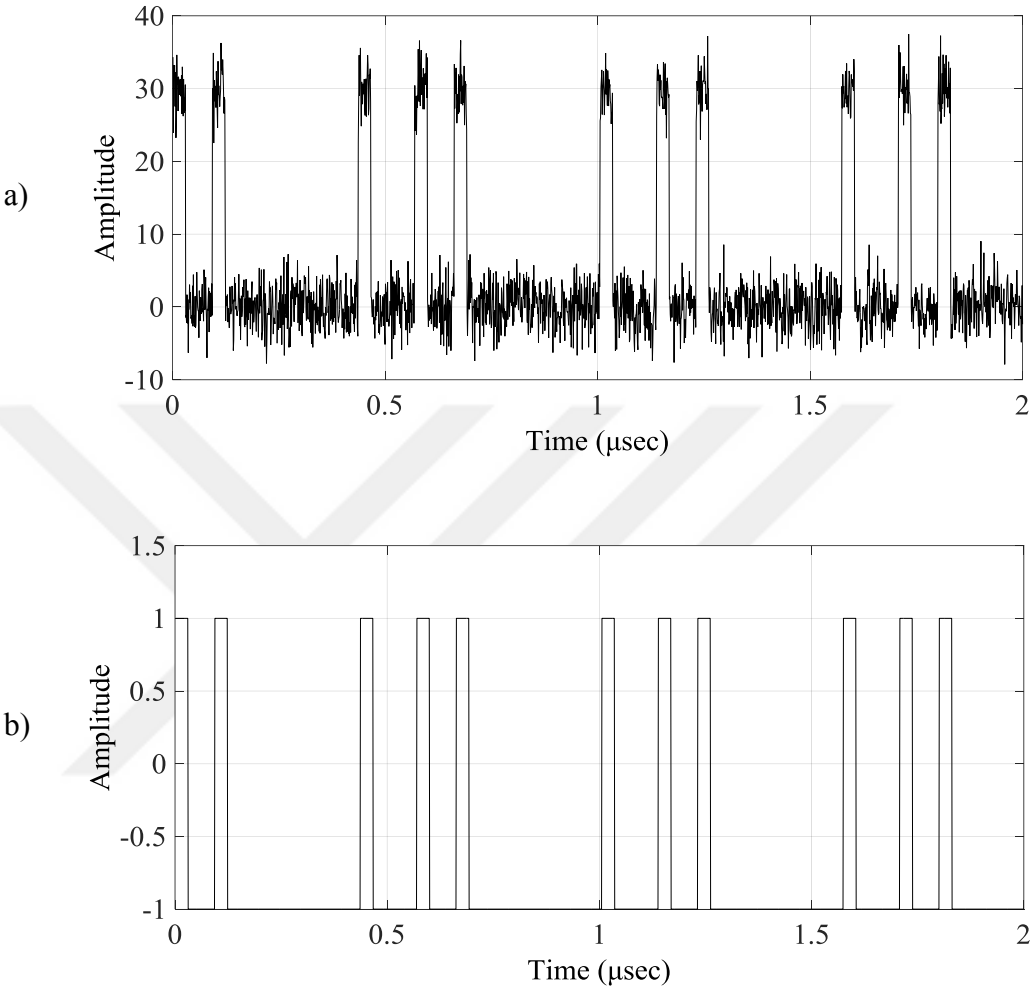

Figure 2.5 Staggered PRI modulation signal a) with Gaussian noise $SNR = 18\ dB$ b) Noise free

2.3.4 Sliding PRI Modulation

In sliding PRI modulation, PRI changes in a monotonically increasing or decreasing behaviour. Sliding, takes place between two extremes of a base sequence, and the base sequence is repeated throughout the main pulse train (Noone, 1999; Wiley, 2006). To simulate such a sliding PRI modulation, we choose the length k of the fixed sequence to be in the range $3 \leq k \leq 10$ randomly for each simulation. So, we define the fixed base set as formulated by (2.6)

$$B_i = r_1 + \frac{i-1}{k-1}(r_2 - r_1) \qquad i = 1,2,\dots,k \tag{2.6}$$

where r_1 and r_2 are the first and last PRIs in the base sequence, randomly chosen for each simulation in the ranges of $50\ \mu sec \leq r_1 \leq 200\ \mu sec$ and $250\ \mu sec \leq r_2 \leq 500\ \mu sec$. The main PRI sequence of length N is then constructed from the base set as expressed by (2.7)

$$X_n^{\mathrm{sl}} = B_{1+\mathrm{mod}_k(n-1)} \qquad n = 1,2,3,\dots,N \tag{2.7}$$

In Figure 2.6, we present a simulated sliding PRI modulation with and without noise.

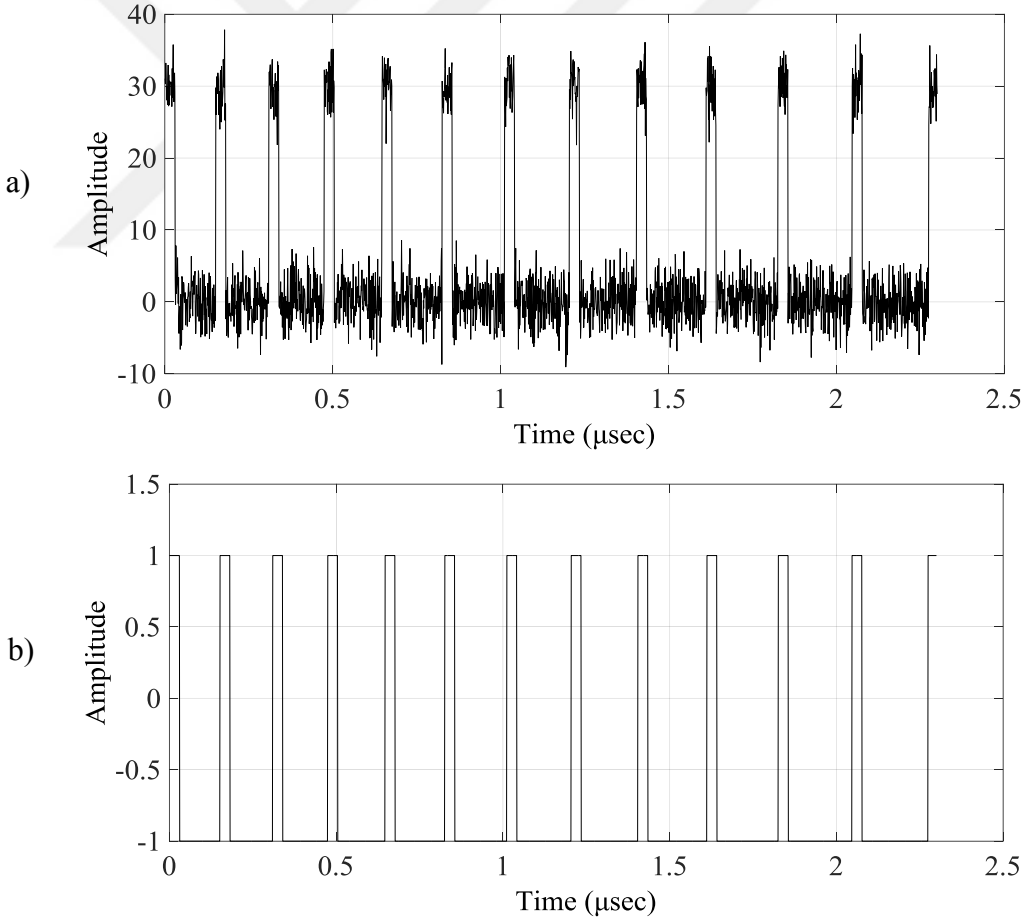

Figure 2.6 Sliding PRI modulation signal a) with Gaussian noise $SNR = 18\ dB$ b) Noise free

2.3.5 Wobulated (Periodic) PRI Modulation

In a wobulated PRI modulation, the PRI is changed sinusoidally around a mean value throughout the pulse train (Noone, 1999; Wiley, 2006). Hence, we write the PRI sequence of length N as represented by (2.8)

$$X_n^{\text{wo}} = r + r_a \sin\left(2\pi \frac{n-1}{r_p - 1}\right) \qquad n = 1,2,\dots,N \qquad (2.8)$$

Here, r is the mean PRI, r_a is the amplitude and r_p is the period of the sine function, which are random integers chosen in the ranges $50\ \mu sec \leq r \leq 500\ \mu sec$, $\lfloor r/5 \rfloor \leq r_a \leq \lfloor r/5 \rfloor$, and $\lfloor N/32 \rfloor \leq r_p \leq \lfloor N/2 \rfloor$. In Figure 2.7, we present a simulated wobulated PRI modulation with and without noise.

a)

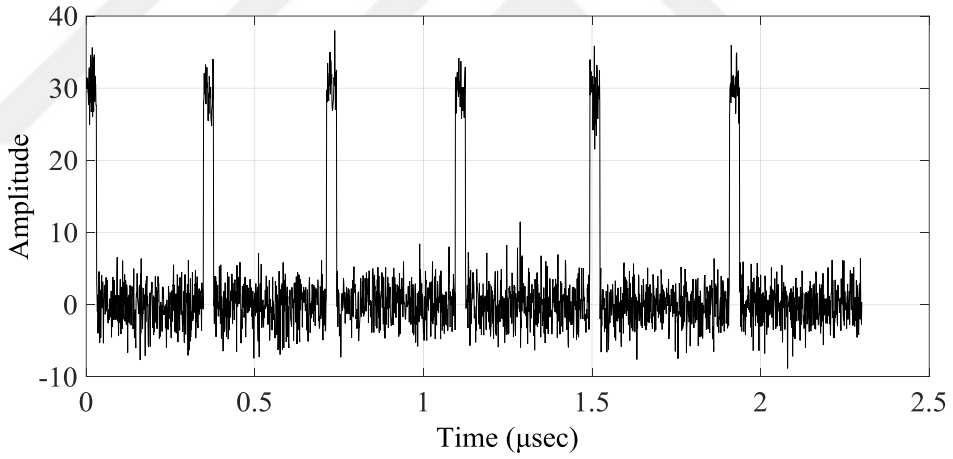

Figure 2.7 Wobulated PRI modulation signal a) with Gaussian noise $SNR = 18\ dB$ b) Noise free

b)

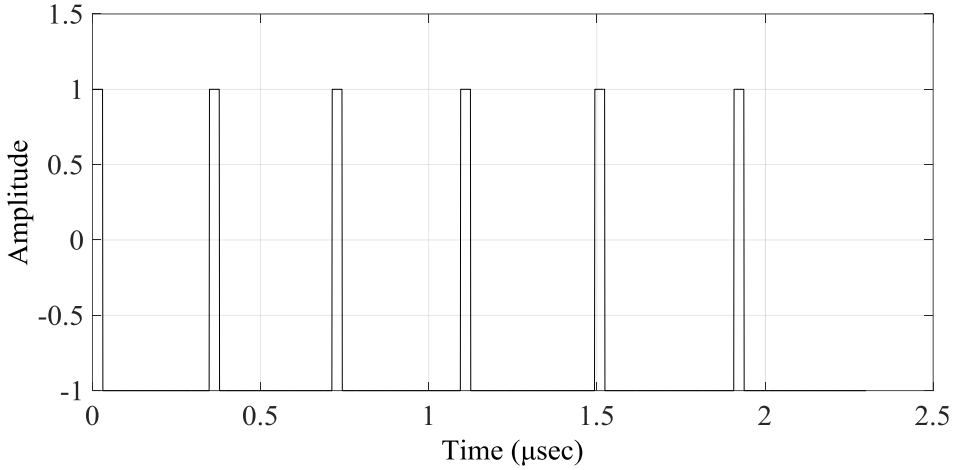

Figure 2.7 continues

2.3.6 Dwell & Switch PRI Modulation

The base sequence in this PRI modulation is initiated by dwelling on a PRI for a number of pulses, and then switching to another PRI. After dwelling on this PRI, it is then switched to another PRI, and so on (Wiley, 2006). The main sequence is constructed by the repetition of the base PRI sequence. Therefore, we construct the base PRI and as represented in (2.9)

$$B_i = \begin{cases} r_1 \quad , & 1 \le i \le k_1 \\ r_2 \quad , & 1 + k_1 \le i \le k_1 + k_2 \\ \vdots & \\ r_M \quad , & 1 + \Sigma_{m=1}^{M-1} k_m \le i \le \Sigma_{m=1}^{M} k_m \end{cases} \tag{2.9}$$

The PRI values are chosen as random integers within the range $50\ \mu sec \le r_m \le 500\ \mu sec$. For each distinct simulation, we randomly determine the lengths of dwells in the range $\lfloor N/32 \rfloor \le k_m \le \lfloor N/16 \rfloor$, for each dwell $\forall m \in \{1,2,\cdots,M\}$, number of which is also randomly determined in the range $3 \le M \le 10$. Here, we can define the length of the base set as $k = \sum_{m=1}^{M} k_m$, and hence the main PRI sequence of length N formulated by (2.10)

$$X_n^{\mathrm{ds}} = B_{1+\mathrm{mod}_k(n-1)} \qquad n = 1,2,3,\dots,N \tag{2.10}$$

In Figure 2.8, We present a simulated dwell & switch PRI modulation with and without noise.

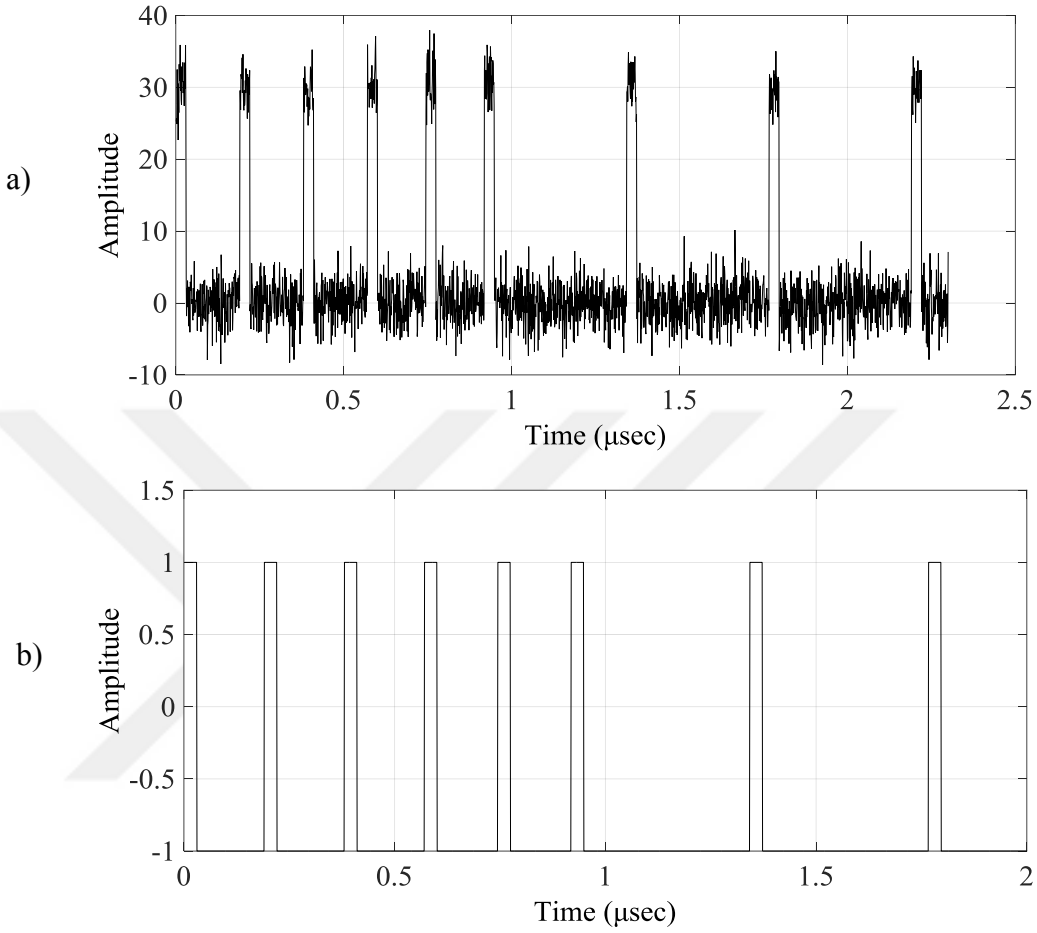

Figure 2.8 Dwell & switch PRI modulation signal a) with Gaussian noise $SNR = 18\ dB$ b) Noise free

In this thesis, we propose a working algorithm for identifying an incoming PRI modulation type as one of the six types described above. Although the constant and staggered PRI modulations can be distinguished during the deinterleaving process (Noone, 1999; Ryoo et al. 2007; Wiley, 2006), other types of PRI modulations are hard to classify, and usually they cannot be distinguished from noise (Ahmadi & Mohamedpour, 1998; Noone, 1999; Kauppi & Martikainen, 2007).

CHAPTER THREE
METHODOLGY

3.1 Basic Methodology

The aim of this section is recognized of PRI by separating from each other's through by using created novel features which is obtained from modulated PRI's mean, autocorrelation, Fourier Transform and Power Spectral Density.

3.1.1 Mean PRI

Mean PRI expressed as in (3.1)

$$\boldsymbol{\mu = \frac{1}{n}\ \sum_{i=1}^{n} a_i = \frac{a_1 + a_2 + a_3 + a_4 + \ldots\ldots + a_n}{n}} \tag{3.1}$$

where a_i is PRI of the nth pulse X_n *which is* received in a pulse sequence having length of N samples.

Deviation of each PRI value from mean of different PRI modulations is presented in Figure 3.1 a-f in frequency domain.

a)

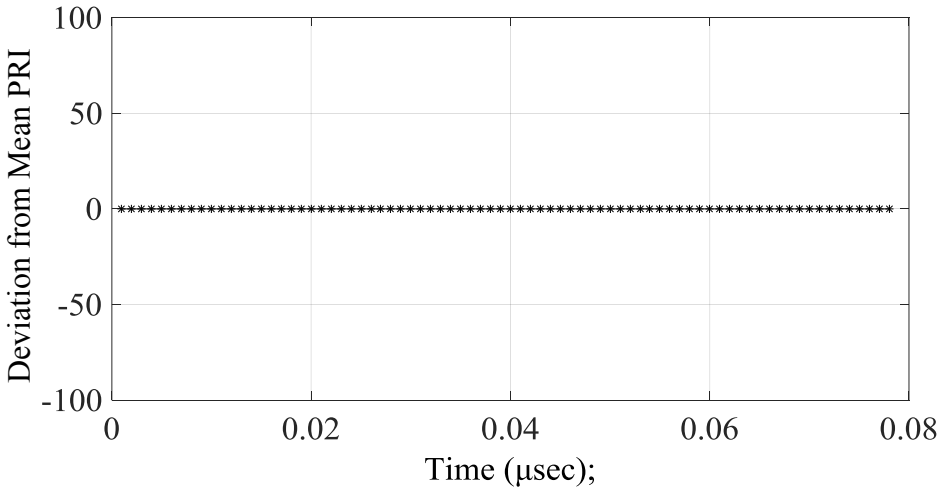

Figure 3.1 Deviation of each PRI value from mean of different PRI modulations: (a) constant, (b) jittered, (c) staggered, (d) sliding, (e) wobulated, and (f) dwell & switch

b)

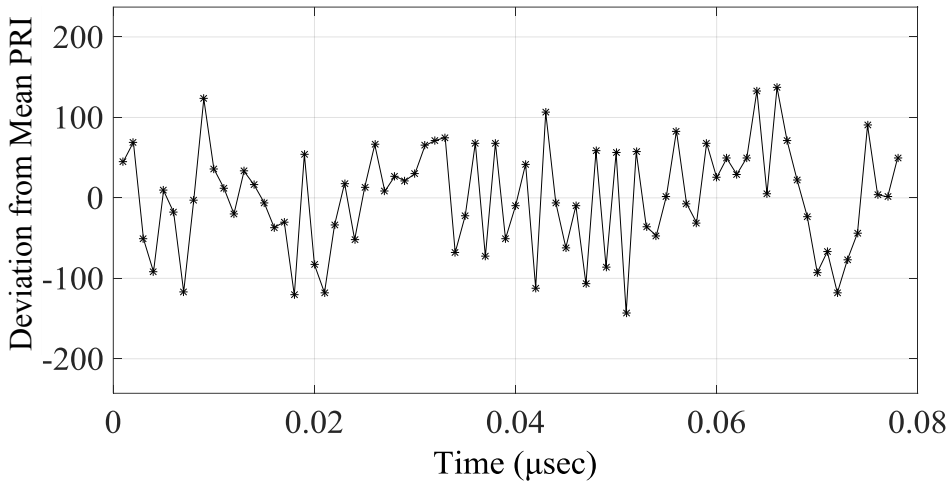

c)

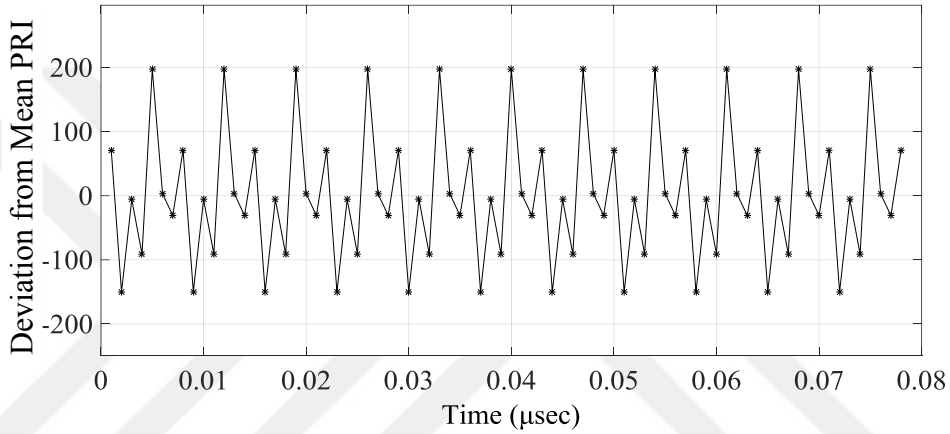

d)

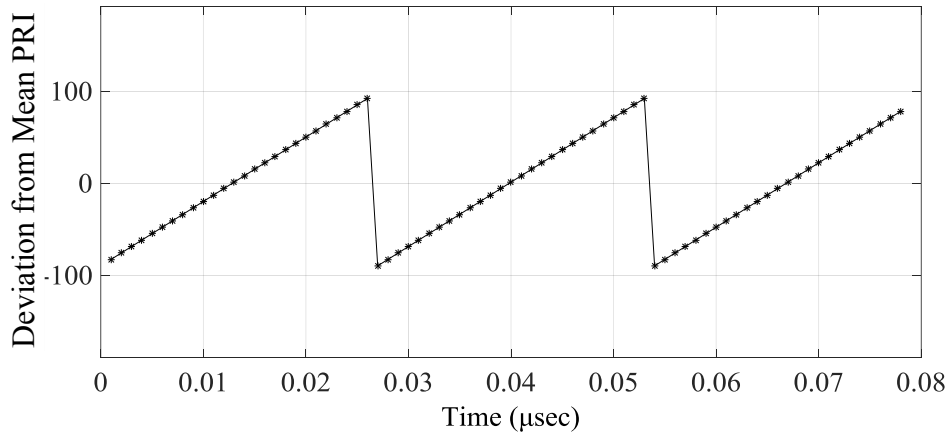

Figure 3.1 continues

e)

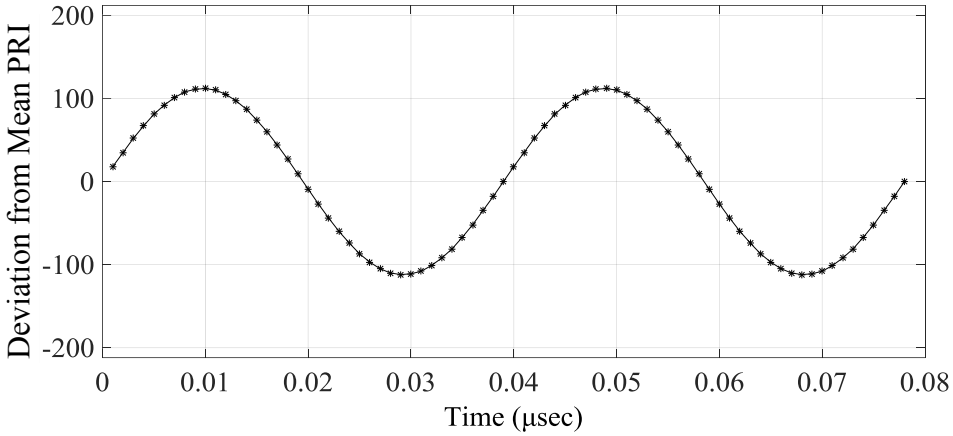

f)

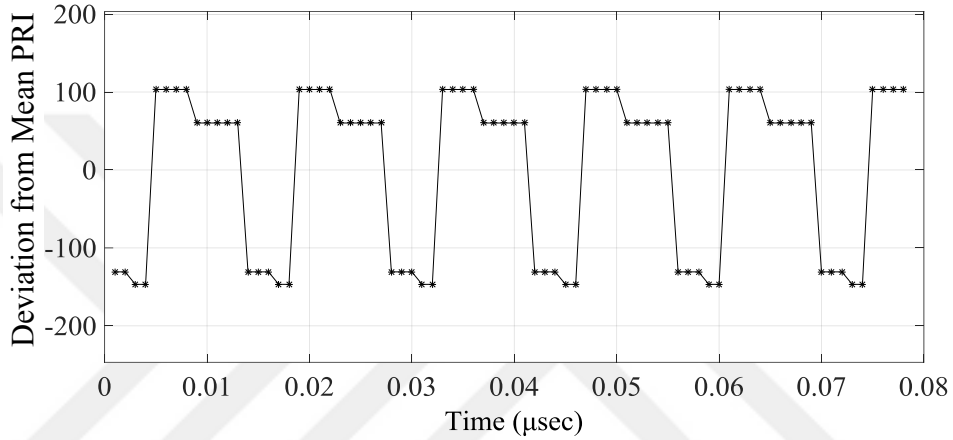

Figure 3.1 continues

Each of the different PRI modulations, plotted in Figure 3.1, are described comprehensively in Refs. (Katsilieris et al. 2017; Hu & Liu, 2010).

3.1.2 Biased Autocorrelation

In PRI modulated signal analysis, autocovariance (r_k) and autocorrelation (u_k) functions are used to characterize the specified PRI type in order to perform feature extraction. These features are based on variation of correlation between values of PRI components at a certain time interval.

Typically, the covariance function is defined as variation of correlation between samples at a lag k, for all different time instants. Under the noisy observation conditions, the autocorrelation function is considered to give statistical information of

a random process such as mean and/or variance that can be used to define random signal in time domain.

Under the ergodicity assumption, sample autocorrelation analysis in PRI modulated data as an effective method of identifying PRI modulation sequences is defined by (3.2) and (3.3) (Broersen, 2006).

$$u_k = \frac{\frac{1}{N}\sum_{n=0}^{N-1-k} X_n X_{n+k}}{\frac{1}{N}\sum_{n=0}^{N-1} X_n^2} \qquad k = 0,1,2,\ldots.K, \qquad n = 0,1,2\ldots\ldots N-1 \quad (3.2)$$

$$u_k = \frac{r_k}{r_0} \quad (3.3)$$

Autocorrelations of different PRI modulated patterns are presented in Figure 3.2 a-f below which are consistent with those studies (Logothetis & Krishnamurthy, 1998) and (Shi et al. 2016).

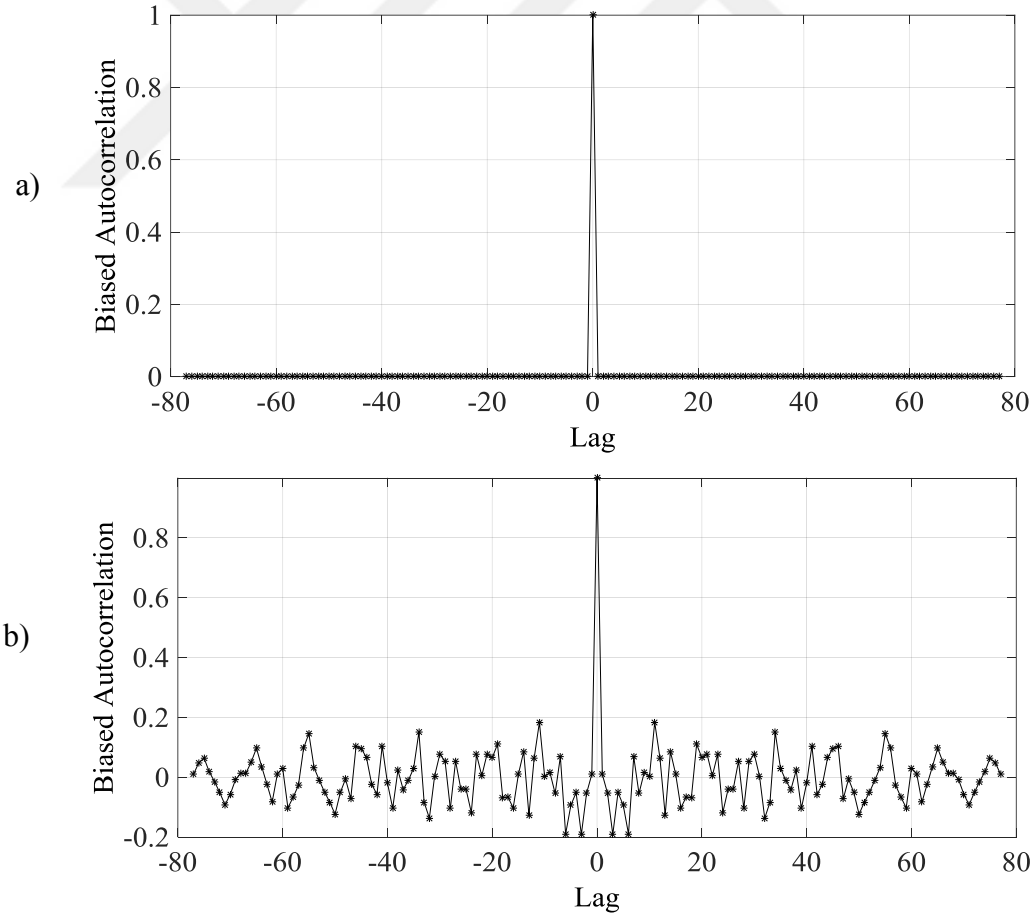

Figure 3.2 Autocorrelation functions of different PRI modulations: (a) constant, (b) jittered, (c) staggered, (d) sliding, (e) wobulated, and (f) dwell & switch

c)

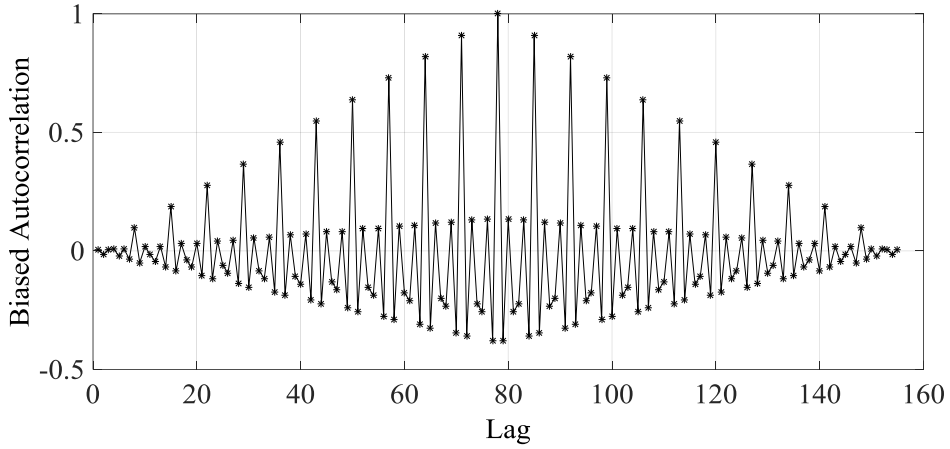

d)

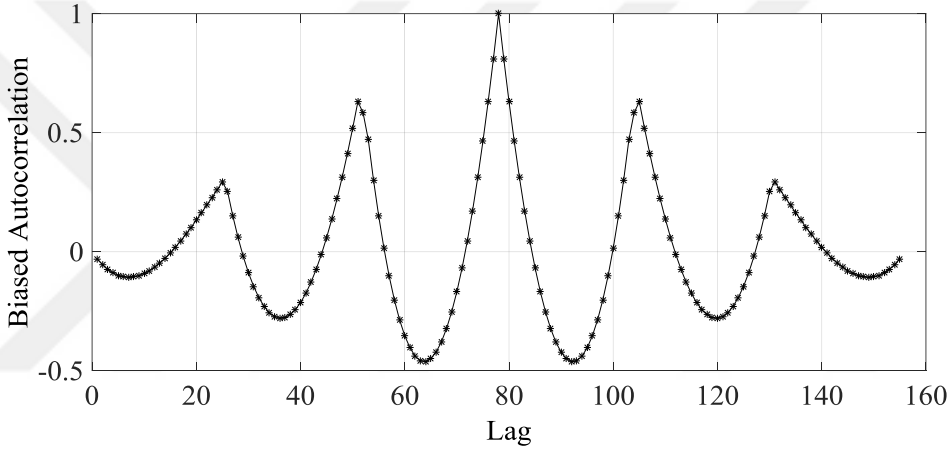

e)

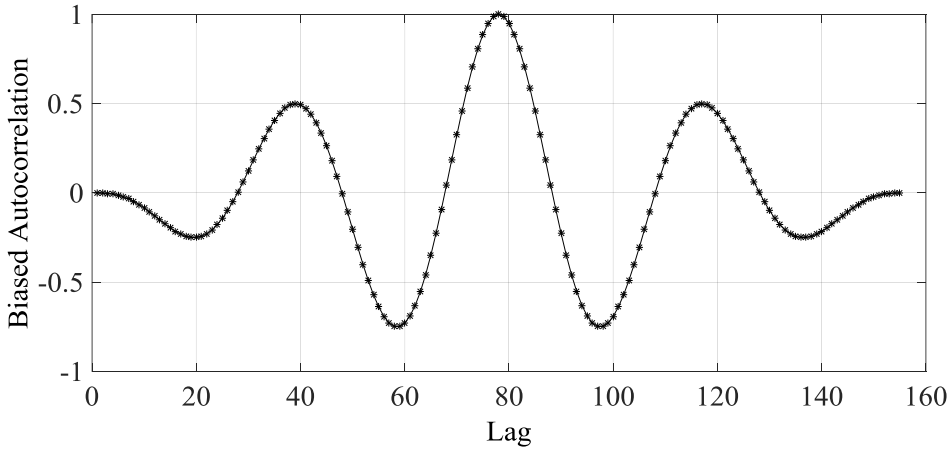

Figure 3.2 continues

f)

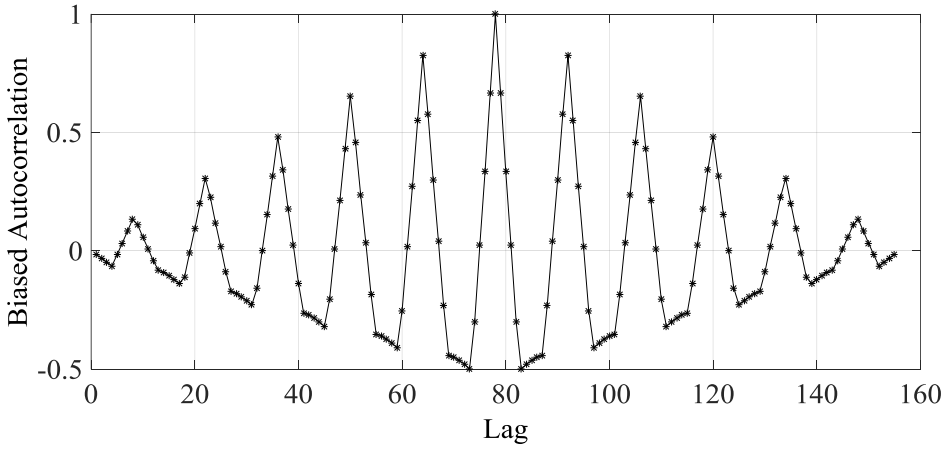

Figure 3.2 continues

It is clearly seen that these functions have distinctive unique signature and they can be considered as potential to characterize each different PRI signal. Alternatively, frequency-based methods can also be utilized due to differing spectral behaviours of each PRI modulated waveforms. In the sequel, spectral characteristics are described.

3.1.3 Fourier Transform and Power Spectral Density

Fourier transformation can be used to analyze any spectral feature of PRI waveform if the PRI pattern has periodic structure. Even though the received signal is usually represented as a function of time, the spectral features also characterize the PRI pattern under investigation.

Due to computational complexity while evaluating the frequency content of a function in practice, the algorithm known as "Fast Fourier Transform (FFT)" is used to extract the spectral content of the observed data which reduces the computation time of a Fourier transformation task, by reducing the number of multipliers. This algorithm is primarily based on Discrete Time Fourier Transform (DTFT) where DTFT of a PRI function X_n is defined by (3.4)

$$F_\omega = \sum_{n=-\infty}^{\infty} X_n \; e^{-j\omega n} \tag{3.4}$$

Fourier transforms of different PRI modulated waveforms are illustrated in Figure 3.3 a-f. One can see that each PRI waveform has a different spectral concentration at different frequencies depending the PRI type.

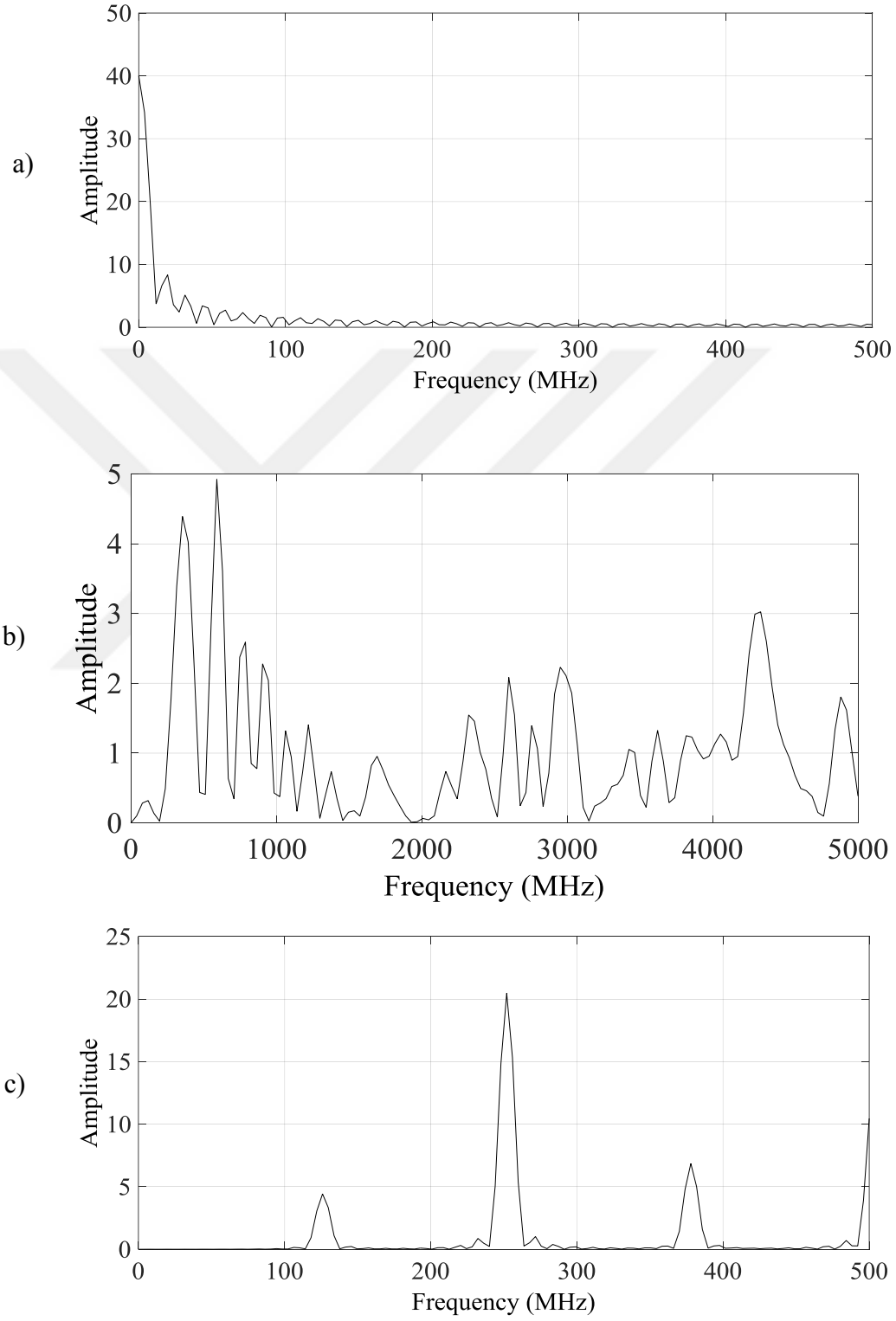

Figure 3.3 Fourier transforms of different PRI modulations: (a) constant, (b) jittered, (c) staggered, (d) sliding, (e) wobulated, and (f) dwell & switch

d)

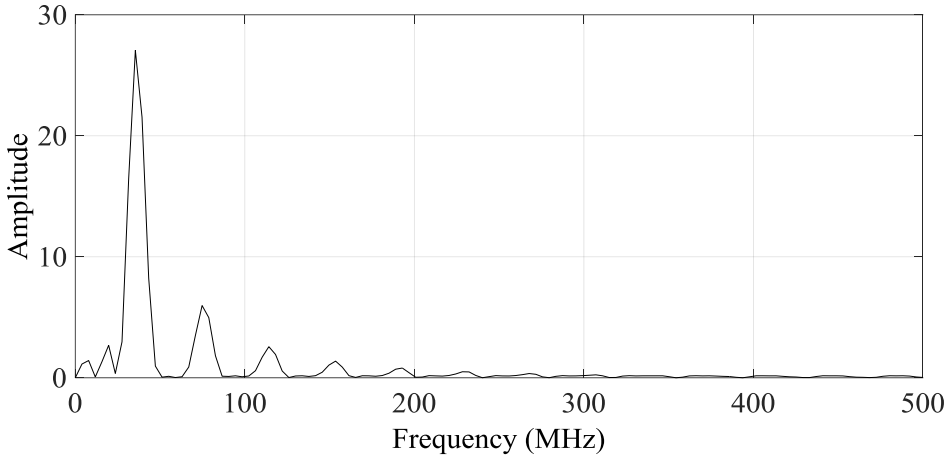

e)

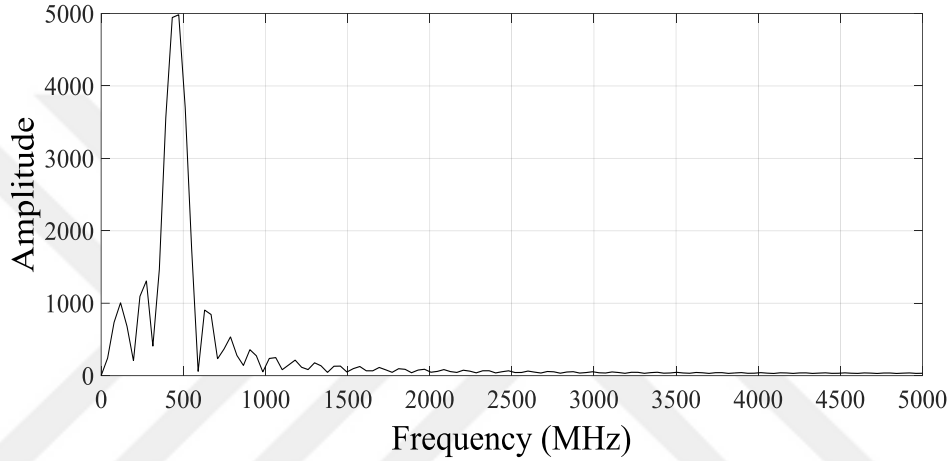

f)

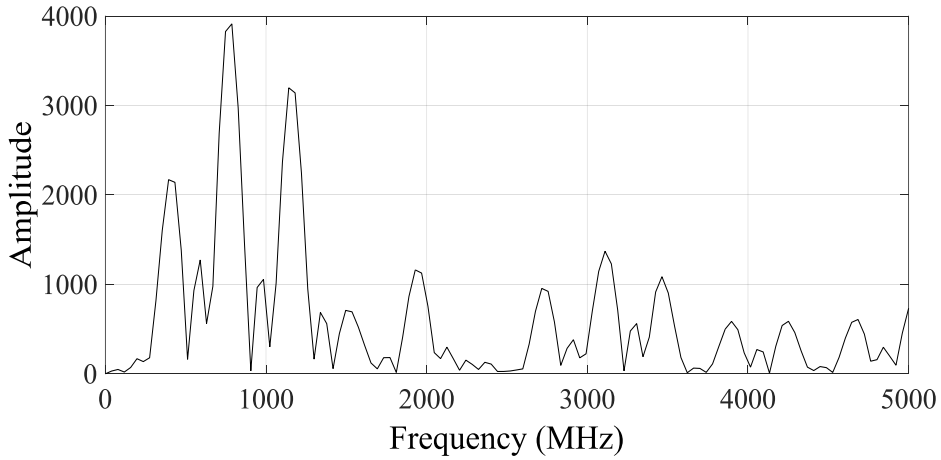

Figure 3.3 continues

In addition to spectral information extracted from direct PRI data, another spectral content obtained from autocovariance function gives feature information that can be used for characterization.

The normalized power spectral density (PSD) can be thought of as the power distribution of the signal over the frequency band. It is defined by (3.5) as the Fourier transform of the autocorrelation function (Stoica & Moses, 2005):

$$PSD(\omega) = \sum_{k=-\infty}^{+\infty} U_k \, e^{-j\omega k} \tag{3.5}$$

Power spectral densities of different PRI modulations are presented in Figure 3.4 below in frequency domains.

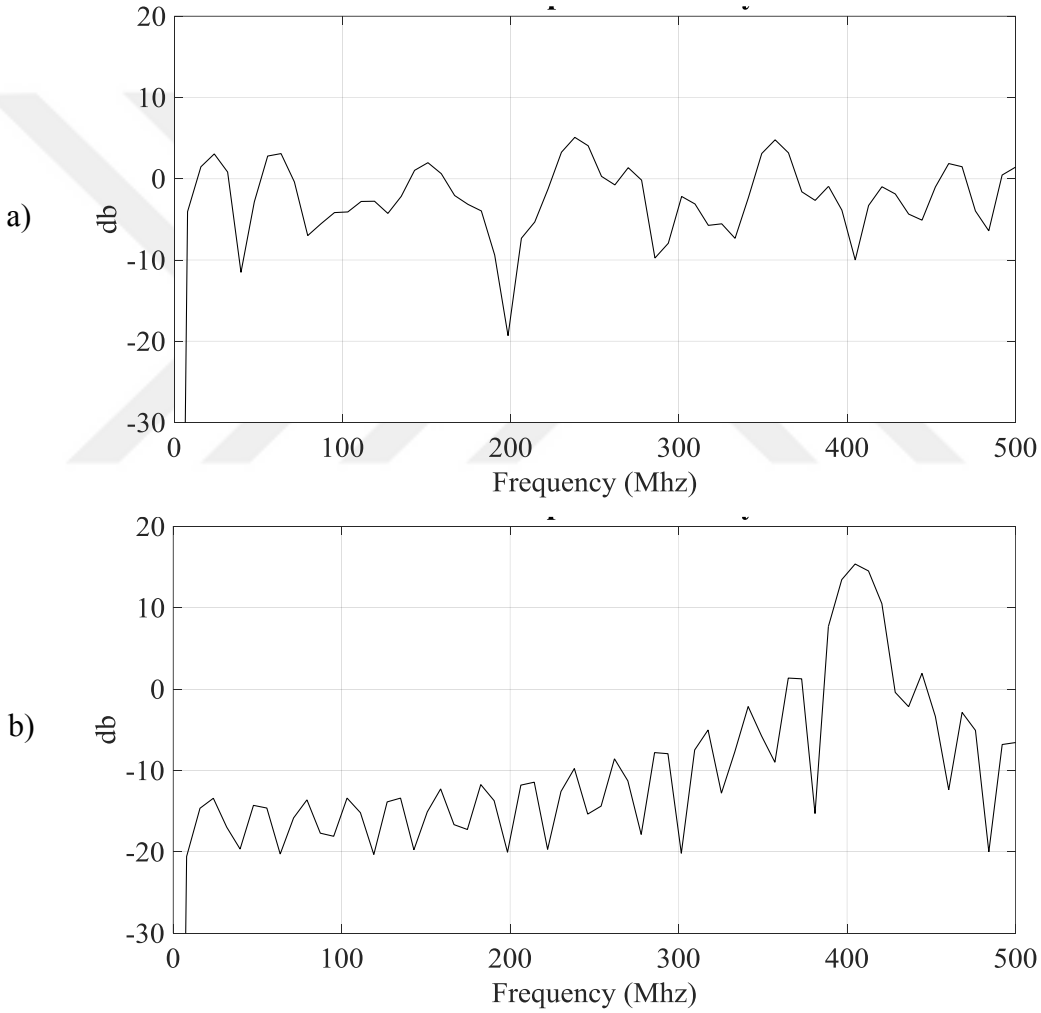

Figure 3.4 Power spectral densities of different PRI modulations: (a) jittered, (b) staggered, (c) sliding, (d) wobulated, and (e) dwell & switch

c)

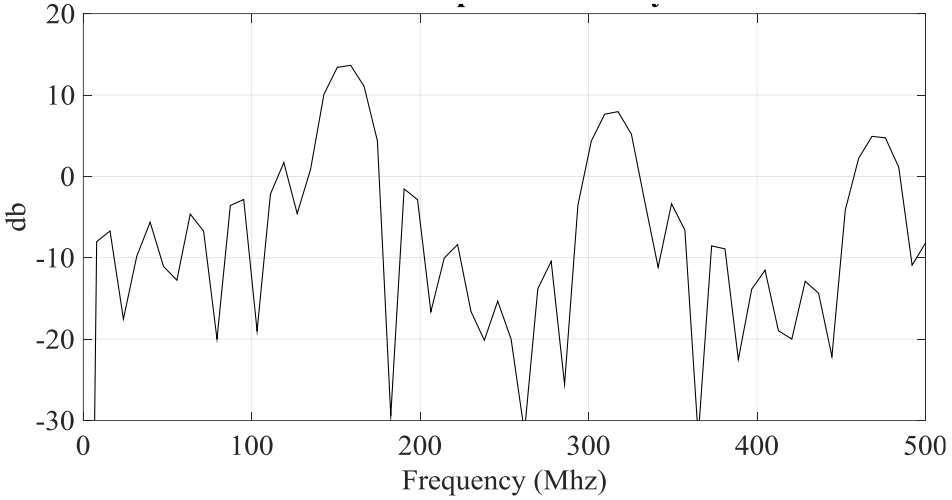

d)

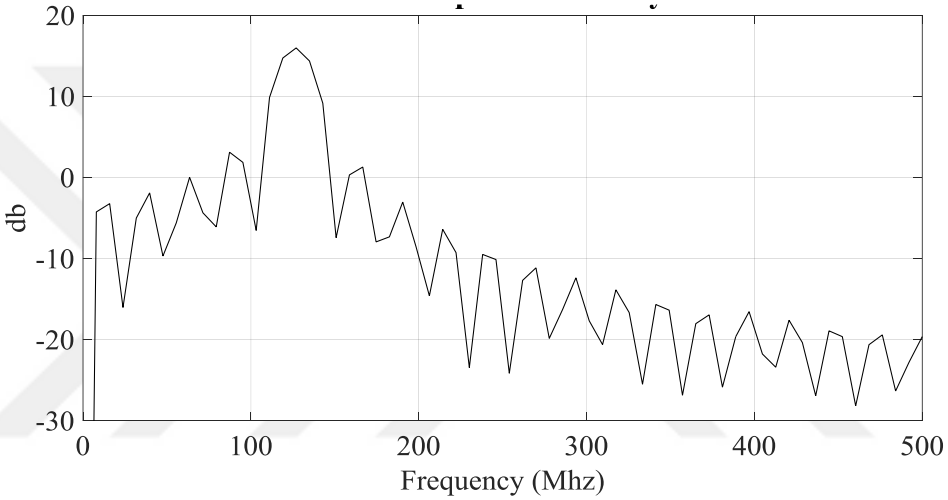

f)

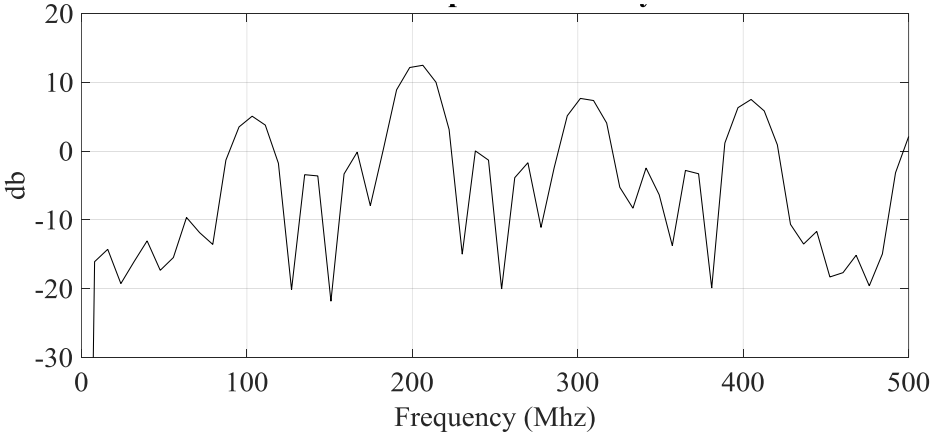

Figure 3.4 continues

3.2 Simulations

MATLAB is chosen as to the simulation environment due to its mathematical applicability and relative ease of use. The algorithms developed in this section have been tested in the MATLAB environment.

Simulations have been developed for each PRI modulation type, and have been run under different and randomly chosen PRI parameters. In each of the simulations, the following procedure is applied:

- Primarily, a signal representing radar pulse sequence is generated.
- White noise is added to the generated signal with different SNR values.
- From this generated signal, the pulse sequence with PRI values is obtained.
- Deviation of each PRI value from mean PRI are determined and the classification-1 is performed by applying feature-1 described below.
- The autocorrelation of the PRI sequence is calculated and the classification-2 is performed by applying feature-2 described below.
- Power spectral density is calculated by the Fast Fourier Transform of the resulting autocorrelation sequence and the classification 3 is performed by applying feature-3 described below.

The simulation results are used to justify the proposed PRI determination and classification algorithms. Different SNR values are applied in simulations, and it is observed that the most suitable SNR values for best classification & determination outputs are in agreement with the applied SNR values in the actual radar environment. The acceptable minimum SNR, depends on the design of the receiver. Generally, for auto-detection with amplitude, TOA, and frequency measurements the setting of an

acceptable minimum S/N is 14 to 18 dB (Avionics Department, 2013). Furthermore, Skolnik expressed that the minimum detectable signal must be sufficient to higher than noise, which is typically by 10 to 20 dB, at the point in the receiver (Skolnik, 1990).

3.2.1 Signal Construction in MATLAB Environment

Rectangular pulse train Y leave a space is characterized by individual pulse function $W_{k,n}$ composed of kth rectangular pulse with amplitude A and fixed length s, which is followed by null vector having variable length X_n for nth pulse given in (3.6):

$$W_{k,n} = \begin{cases} A\ , & (n-1)s + \sum_{j=1}^{n-1} X_j \le k \le ns + \sum_{j=1}^{n-1} X_j \\ 0\ , & ns + \sum_{j=1}^{n-1} X_j < k \le ns + \sum_{j=1}^{n} X_j \end{cases} \tag{3.6}$$

where $n = 1,2, \ldots, N$. Note that $X_0 = 0$. The rectangular pulse and following null signal for nth pulse is simply expressed by Y_n as a component of pulse train Y. The total length of the pulse train Y is defined by (3.7)

$$L = Ns + \sum_{n=1}^{N} X_n \tag{3.7}$$

In presence of noise represented by noise sequence S, the local received signal R_n which is defined (3.8) for nth pulse is observed at the receiver input as:

$$R_n = Y_n + S \tag{3.8}$$

A typical jittered PRI modulated signal R with A=18 in presence of additive white Gaussian noise with SNR=18 dB is shown in Figure 3.5. The amplitude $A/2$ is indicated as the horizontal line which is considered as reasonable threshold value

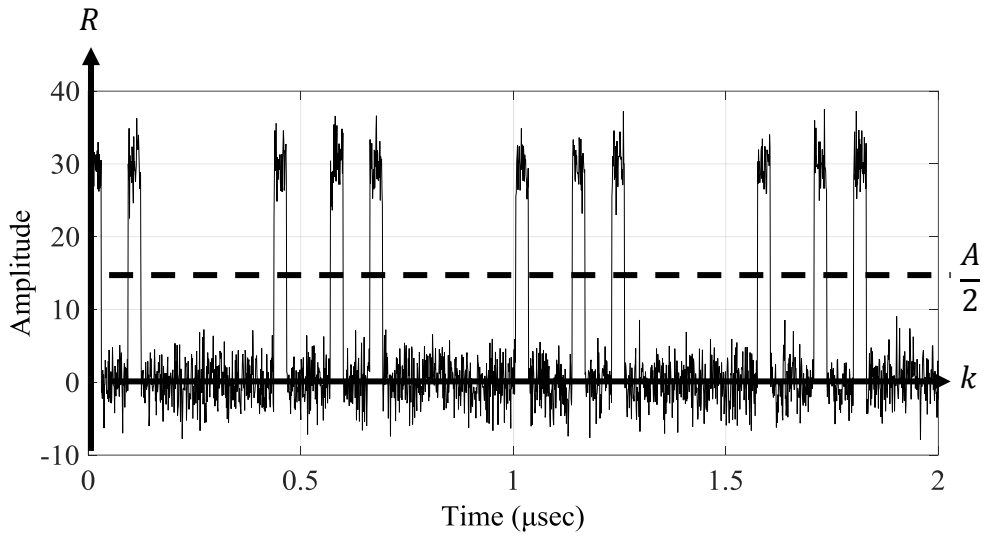

Figure 3.5 A typical noisy jittered PRI modulated pulse train, $A = 30, SNR = 18\ dB$

The SNR is expressed in terms of as dB by (3.9)

$$SNR\ (dB) = 10\ log \frac{P_{signal}}{P_{noise}} \tag{3.9}$$

where P_{signal} is the average signal power and P_{noise} is the noise power, both of which are measured in units of watts.

In order to determine the signal-to-noise ratio SNR, the Gaussian noise is considered to have power N_0 and SNR can be defined for rectangular pulsed signal as (3.10)

$$SNR = \frac{P_{signal}}{P_{noise}} = 10 \log \frac{A^2}{N_0} \tag{3.10}$$

Considering the noise having zero –mean, the power directly corresponds to its variance and the relation with variance can be established as $\sigma^2 = \frac{N_0}{2}$. The noise variance can be determined as $\sigma^2 = \sqrt{\frac{P_{avg}}{2\,(10^{\frac{SNR}{10}})}}$ and S, which is obtained from $SNR\ (db)$, is presented by (3.11):

$$S \sim \mathcal{N}(0, \sigma^2) \tag{3.11}$$

It is only interested in the ordering of the consecutive pulse intervals under noise contamination, there a new time series Z is obtained from the observed noisy data signal by a signum function as expressed by (3.12)

$$\mathrm{Z} = sgn(\mathrm{R} - \mathrm{A}/2) \tag{3.12}$$

The signum function for each pulse interval change can be defined as (3.13)

$$Z = \begin{cases} 1 & , R > A/2 \\ 0 & , R < A/2 \end{cases} \tag{3.13}$$

Practically, determining transition points from 0 to 1, PRI sequence (X_i for $i = 1,2, \dots, N$) can be achieved.

3.3 Feature Selection

Once the PRI data is obtained under noise free environment or estimated under additive noise, the features can be extracted to recognize PRI modulations. The main goal is to recognize common PRI modulation types given in Section 2.3. For this purpose, the features are extracted both in terms of statistical properties of PRI data or the raw PRI data itself. Here, the motivation comes from the fact that the features can be extracted from almost any pulse sequence rather than PRI data. The distinctive requirement is to be able to have a potential satisfactory separation capability among the wide variety of feature set as much as possible.

Statistical properties potentially carry significant intrinsic information in order to extract distinguishable feature among different PRI data. In the sequel, the methods to extract three features are described.

3.3.1 Feature-1: Deviation of each PRI value from mean PRI

The aim of this feature is to characterize the PRI sequence by normalizing the PRI sequence and subtracting each PRI X_n from the mean PRI value $\langle X \rangle$, and distinguishing the PRI modulation by subjecting the resulting sequence to the classification criteria specified in feature-1.

First, the deviation of each PRI value from the mean PRI is calculated by (3.14):

$$m_n = X_n - \langle X \rangle \qquad n = 1,2,\dots N \tag{3.14}$$

Then a sequence of ones and zeroes (M) is constructed from this deviation sequence, which is defined by (3.15)

$$M_n = \begin{cases} 0\ , & |m_{n+2}| - |m_{n+1}| = |m_{n+1}| - |m_n| \\ 1\ , & else \end{cases} \qquad n = 1,2,\dots,N-2 \tag{3.15}$$

Finally, feature-1 (f_1), which is formulated by (3.16), is constructed as the number of ones in the sequence M, normalized by the number of elements in M.

$$f_1 = \frac{1}{N-2}\sum_{n=1}^{N-2} M_n \tag{3.16}$$

In Figure 3.6, we present the variation of f_1 for six types of PRI modulations, each with 100 realizations of different randomly chosen parameters used to characterize each PRI type. In all simulations SNR value is taken as $18\,db$ which is reasonable value to analyze the data. It is observed $f_1 < 0.05$ for constant, $0.05 \leq f_1 < 0.35$ for sliding PRI. More generally these two PRI patterns are collected to be $f_1 < 0.35$ for constant and sliding PRI modulations. This serves as the first step of classification algorithm. Furthermore, it is also observed that $f_1 > 0.95$ for most of the data belonging to jittered and staggered PRI modulations.

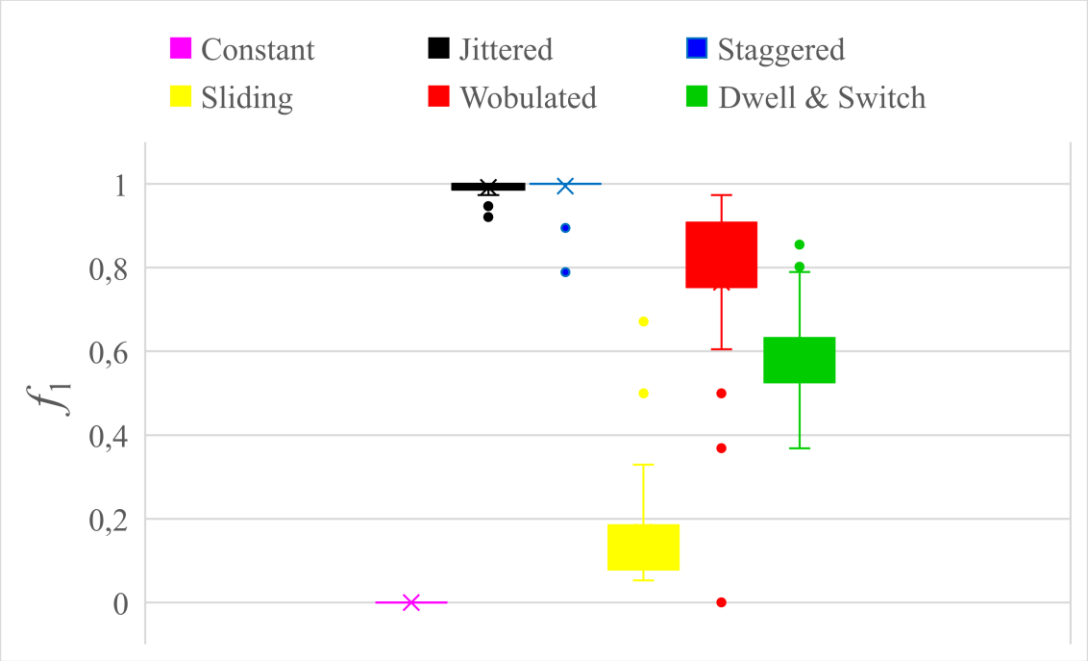

Figure 3.6 Variation of f_1 for six types of PRI modulations, each with 100 realizations of different randomly chosen parameters at $SNR = 18\ dB$

3.3.2 Feature 2: Comparison of Consecutive Values of Autocorrelated PRI Sequence

Autocorrelation is significant when determining the overall statistics of the different PRI modulation types. However, direct discrimination of wobulated PRI, dwell & switch PRI, and sliding PRI from only autocorrelation value is found not to be possible. Fortunately, it is observed that autocorrelation results are more discriminative to separating staggered PRI and jittered PRI sequences from the other PRI modulations. To obtain the second feature f_2, autocorrelation of the PRI sequence (c_k) is calculated by (3.17).

$$c_k = \frac{\sum_{n=1}^{N-k} m_n m_{n+k}}{\sum_{n=1}^{N} m_n^2} \qquad k = 0,1,2,\ldots,N-1 \qquad (3.17)$$

Once the autocorrelation is evaluated, a new time series K is obtained. According to this approach, if two consecutive elements of the autocorrelation sequence are both positive or both negative, then the corresponding K value is 1, and it is 0 otherwise

(*i.e.*, for consecutive elements of the autocorrelation sequence having different signs). K_n is defined by (3.18).

$$K_n = \begin{cases} 1\ , & c_n \geq 0 \ \text{ and } \ c_{n+1} \geq 0 \\ 1\ , & c_n < 0 \ \text{ and } \ c_{n+1} < 0 \\ 0\ , & \text{otherwise} \end{cases} \qquad n = 1,2,\ldots,N-1 \quad (3.18)$$

The mean number of ones in the array K gives the second feature f_2 and is expressed by (3.19).

$$f_2 = \frac{1}{N-1}\sum_{n=1}^{N-1} K_n \qquad n = 1,2,\ldots,N-1 \quad (3.19)$$

In Figure 3.7, it is presented the variation of f_2 for six types of PRI modulations, each with 100 realizations of different randomly chosen parameters at $SNR = 18\ db$ (same as those in Figure 3.6). By using the f_2, the rest of the four types PRI patterns can be classified into two categories as jittered and staggered ($f_1 > 0.95$) in one category, while wobulated and dwell & switch ($f_1 < 0.95$) in another category. Here, in Figure 3.7, it is observed that f_2 is not capable of further classification of different PRI modulations although it offers different local intervals for jittered and staggered PRI patterns. For further analysis, another feature f_3, is proposed to construct a complete feature region than can be discriminated using classifiers in the literature.

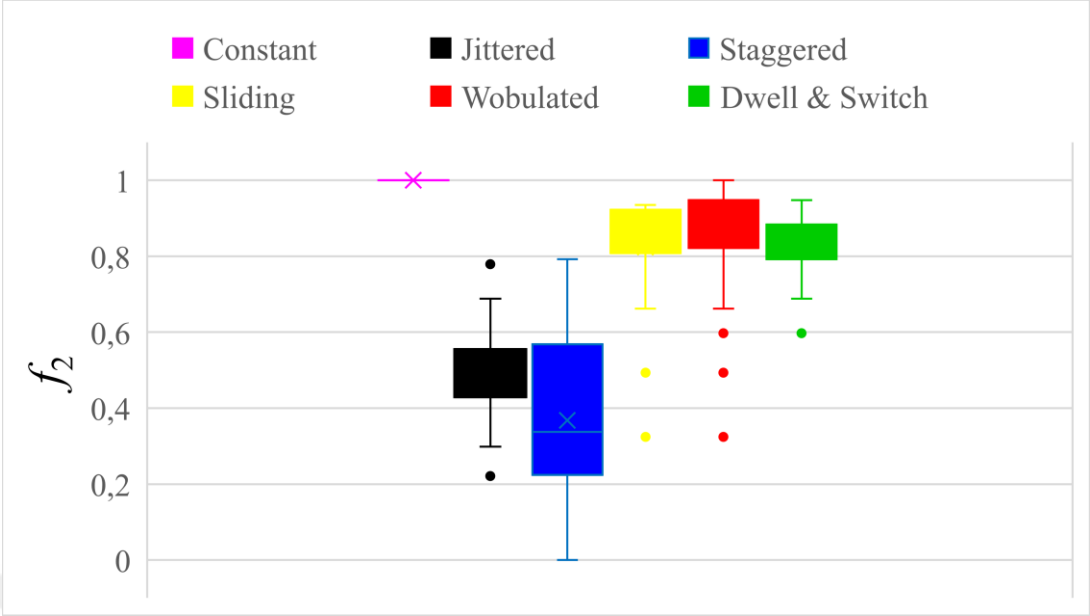

Figure 3.7 Variation of f_2 for six types of PRI modulations, each with 100 realizations of different randomly chosen parameters at $SNR = 18\ dB$

3.3.3 Feature 3: Maximum Value of Power Spectral Density

The power spectral density is an effective feature that can be used to distinguish different types of autocorrelated PRI sequences. The third feature f_3, calculates the maximum peak value of the power spectral density obtained from the c_n autocorrelation sequence as calculated by the FFT calculated by (3.20).

$$f_3 = \max\left(|FFT(c_n)|\right) \tag{3.20}$$

where $FFT(\cdot)$ denotes the Fast Fourier Transform operation. In Figure 3.8, it is presented the variation of f_3 for six types of PRI modulations, each with 100 realizations of different randomly chosen parameters at $SNR = 18\ dB$ (same as those in Figures 3.6 and 3.7). In Figure 3.8, it is observed that f_3 roughly divides PRI types into three categories where the first category is composed by wobulated PRI, the second class is collected as staggered, sliding, dwell & switch, the third class is approximately constant and jittered PRI patterns.

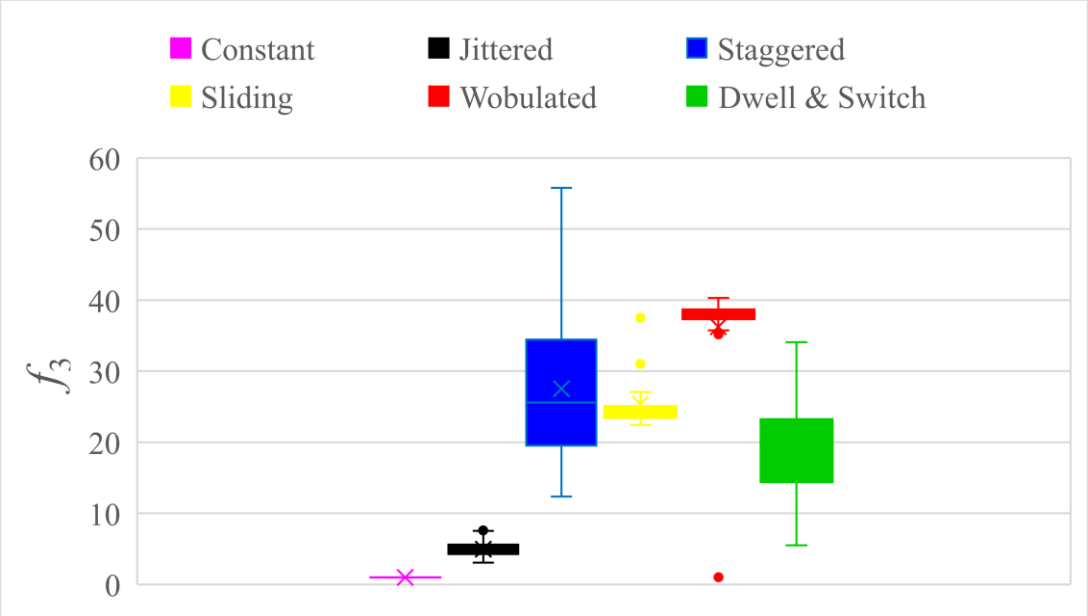

Figure 3.8 Variation of f_3 for six types of PRI modulations, each with 100 realizations of different randomly chosen parameters at $SNR = 18\ dB$

3.3.4 Compilation of PRI Patterns in Features Space

Although all of the features cannot give a satisfactory discrimination performance individually, the set of features in increased dimension is observed in this section. Figure 3.9 (a) and (b) shows the combined values of three features for 100 distinct simulated signals with randomly chosen parameters for all six types of PRI modulations. It should be remarked that the features f_1 and f_3 have a notable impact on generating discriminative PRI patterns. According to these results, once the two features f_1 and f_3 are calculated, PRI modulated patterns can be approximately classified by applying appropriate threshold to these feature values. One can consider an approximate decision boundary in terms of each feature itself by inspection. Firstly, f_1 derived from the mean PRI, is restricted to be $f_1 < 0.05$ for constant PRI modulation, and $0.05 \leq f_1 < 0.35$, for sliding PRI modulation. However, if this feature $0.35 < f_1 < 0.95$, it may be either wobulated or dwell & switch PRI modulation, while for $f_1 > 0.95$, it may be either jittered or staggered PRI modulation. The feature f_3, derived from the PSD of the autocorrelation of the mean PRI sequence, if $15 < f_3 < 40$ it is dwell & switch, and if $f_3 \geq 40$ it is wobulated for the selection

of $0.35 < f_1 < 0.95$. If $f_3 < 15$ it is jittered, and if $f_3 \geq 15$ it is staggered for the consideration of $f_1 > 0.95$.

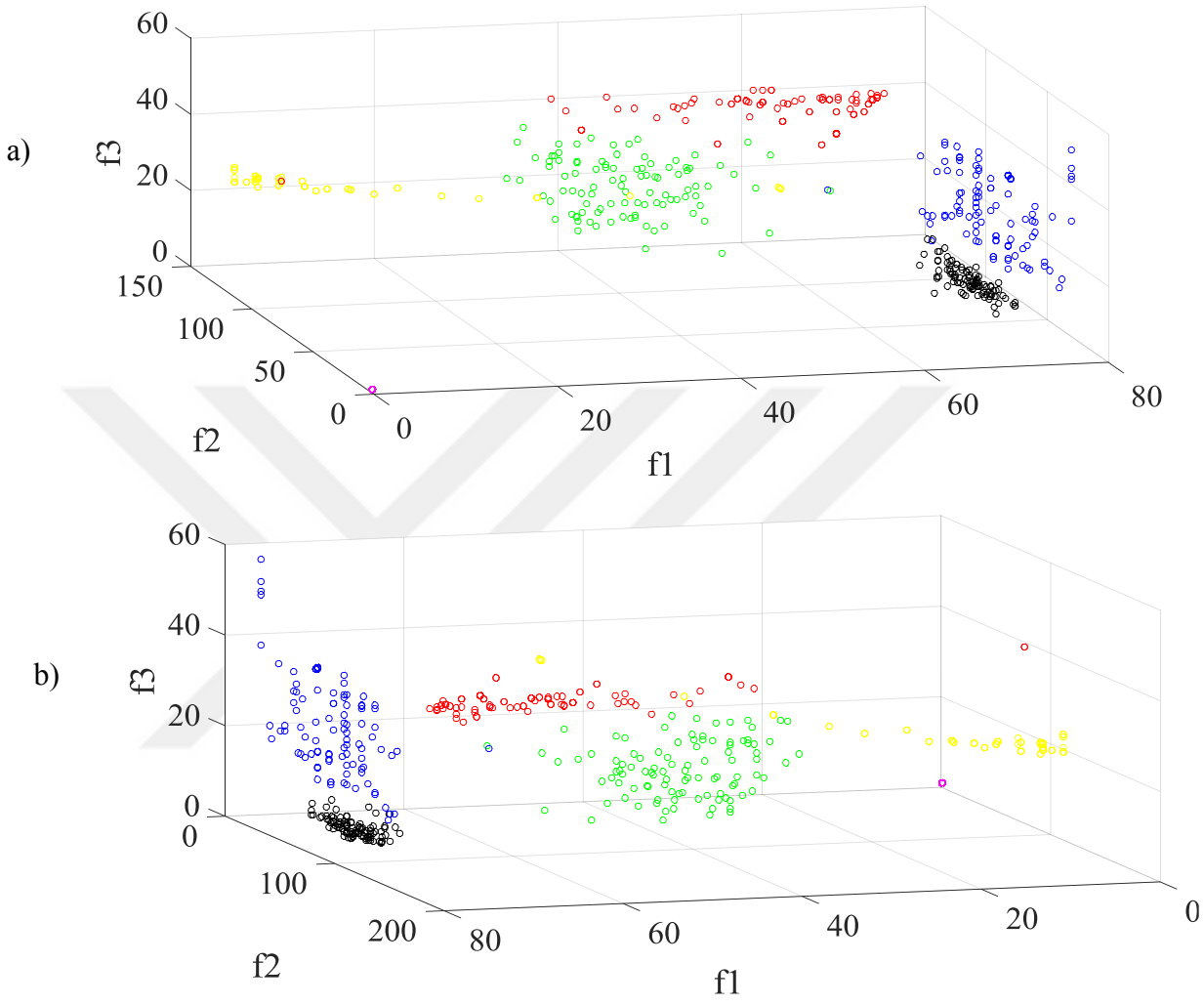

Figure 3.9 (a) and (b): Feature values for 100 distinct simulated signals with randomly chosen parameters for all six types of PRI modulations. Same colour code as in Figures 3.6-3.8

The approximate decision block diagram is given as a block diagram shown in Figure 3.10 below. It should be noted that there can be constructed an improved classification performance by applying classification methods such as support vector machine, artificial neural networks which are listed as literature search in the next section.

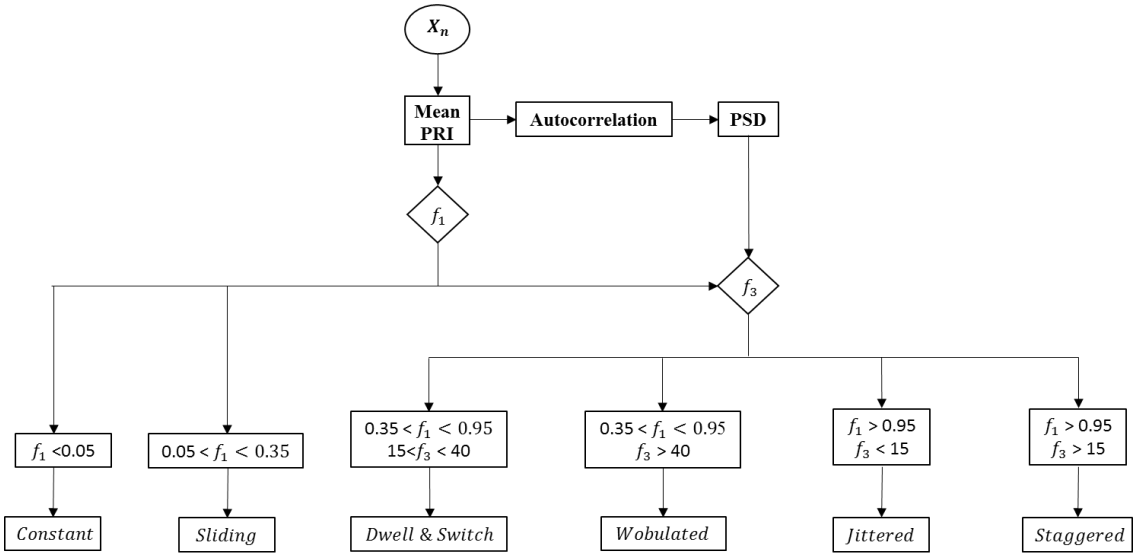

Figure 3.10 PRI classification algorithm according to the features, f_1 and f_3

As can be observed from Tables 3.1, 3.2, the proposed classification algorithm cannot give satisfactory results for 15 dB but the correct classification ratio increases for higher SNR vlaue as 18 dB. Therefore, the feature selection algorithm needs to be improved in order to ensure robustness against noise for lower SNR values. Nevertheless, It is also noted that typical radar environments have SNR range.

Table 3.1 Classification percentages for different PRI modulations at SNR = 15 dB

$\boldsymbol{SNR = 15db}$		Generated Signal					
		Constant	Jittered	Staggered	Sliding	Wobulated	Dw & Sw
As Classified Signal	Constant	**89.30%**	0.00%	0.00%	0.00%	0.33%	0.00%
	Jittered	0.00%	**97.70%**	25.80%	0.00%	0.00%	0.00%
	Staggered	0.00%	0.00%	**71.80%**	0.00%	0.97%	0.04%
	Sliding	0.70%	0.00%	0.00%	**86.60%**	0.01%	0.00%
	Wobulated	0.00%	0.00%	0.00%	0.00%	**82.40%**	0.00%
	Dw & Sw	10.70%	0.00%	0.15%	11.50%	10.40%	**73.20%**
	Unclassified	0.00%	2.20%	2.25%	1.90%	8.89%	26.76%

Table 3.2 Classification percentages for different PRI modulations at SNR = 18 dB

$SNR = 18\ db$		Generated Signal					
		Constant	Jittered	Staggered	Sliding	Wobulated	Dw & Sw
As Classified Signal	Constant	**99.80%**	0.00%	0.00%	0.00%	0.53%	0.00%
	Jittered	0.00%	**96.50%**	0.63%	0.00%	0.00%	0.32%
	Staggered	0.00%	0.00%	**91.70%**	0.00%	0.67%	0.25%
	Sliding	0.02%	0.00%	0.00%	**89.40%**	0.01%	0.03%
	Wobulated	0.00%	0.00%	0.02%	0.00%	**85.90%**	0.06%
	Dw & Sw	0.00%	0.00%	0.15%	10.60%	0.29%	**89.64%**
	Unclassified	0.18%	3.50%	7.50%	0.00%	12.63%	9.63%

Although it is demonstrated in (Liu & Zhang, 2017) that PRI modulated signals are classified with 99% accuracy, this method does not consider staggered PRI. PRI modulation classification except the staggered one is also applied in other methods, (Conroy & Moore, 1998) and (Orsi, Moore & Mahony, 1999). Indeed, separation of staggered PRI from other modulation types with high accuracy is reported to be the most problematic classification (Conroy & Moore, 1998; Mahdavi & Pezeshk, 2010). Although correct classification percentages higher than the method proposed in this thesis exist, these are realized with multi-layer perceptron networks (Kauppi & Martikainen, 2007), and such high values expressed to be obtained in the absence of noise.

3.4 Other PRI Recognition and Classification Techniques:

3.4.1 Classification

In this section, other methods for PRI classification in the literature are briefly explained. These methods are summarized as correlation-based classification (Shi et al. 2016; Katsilieris et al. 2017), using multilayer perceptron (Noone, 1999),

(Kauppi & Martikainen, 2007), wavelet transform based feature extraction (Gençol et al. 2016). Similarly, PRI sequences are recognized in terms of time-frequency domain (Hu & Liu, 2010). Alternatively, hierarchical clustering method by (Ahmadi & Mohamedpour, 1998) is aimed of PRI recognition. As a different problem description, (Ghani et al. 2016) analyzed spurious and missing pulses in PRI modulated signals. In a recent study, decimated Walsh-Hadamard transform is used for PRI analysis (Ghani et al. 2017).

3.4.2 Recognition

PRI recognition by using the features calculated from the autocorrelation of the PRI sequences are explained by (Ryoo et al. 2007). However, since these features are highly sensitive to signal imperfections, it is reported that missing pulses were compensated and spurious pulses are removed prior to recognition process.

(Kauppi & Martikainen, 2007) used a neural network classifier, PRI modulations are divided into three groups as first step. Then, using one-dimensional classifiers, these groups are further binary classified. Some of the suggested features in the procedure given by (Kauppi & Martikainen, 2007) used sequential difference (SDIF) histograms in order to deinterleaving (Milojevic & Popovic, 1992).

CHAPTER FOUR
ROBUST ESTIMATION UNDER NON-GAUSSIAN NOISE

The literature related with PRI analysis, the effect of noise contaminating to rectangular pulses is not of interest in common or the SNR is assumed to be sufficiently large to observe pulse onset without any notable time delay. However, the noise causes PRI patterns to deviate from their actual values. Moreover, any non-Gaussian noise, which is generally modelled to be impulsive, may cause spurious pulses yielding different PRI pattern than actual one. Therefore, SNR is crucial in PRI characterization. Within the PRI recognition problem, the time-of-arrival depends on the detection of correct pulses where the rising edge of the rectangular pulses should be correctly detected. The correct detection of the rising edge of a pulse strongly misleading for low SNR. The impulsive character of noise may be due to channel effects and/or jammers, which results in heavy-tailed noise distribution. The observed signal under impulsive noise can be erroneously detected at time instants of rising edges of pulses. The effect of impulsive α −stable noise on radar signal processing are investigated in earlier studies (Zaimbashi et al. 2013; Aalo et al. 2015)

This chapter is primarily based on detection of pulses under impulsive noise in order to reconstruct PRI patterns and developing methods to overcome degrading effect of noise using robust estimators as the contribution. The impulsive noise is properly modelled with α −stable distributed noise. In the sequel, the α −stable distribution is explained briefly with its important features.

4.1 Alpha-Stable Distribution

Among the several formal definitions “alpha-stable distribution” or “stable distribution” is defined as follows (Arce, 2005): Any random variable X is said to have stable distribution if the following equality given by (4.1) is hold

$$AX_1 + BX_2 = CX + D \tag{4.1}$$

where A, B, C are positive numbers and D is any real number, X_1 and X_2 are independent copies of X, "=" corresponds to equality in terms of distribution. The probability density function $f(x)$ of α −stable distribution is expressed by (4.2), in terms of its characteristic function $\varphi(\theta)$.

$$f(x) = \frac{1}{2\pi}\int_{-\infty}^{\infty} \varphi(\theta)\, e^{-jx\theta}\, d\theta. \tag{4.2}$$

Since there is no closed form expression of $f(x)$ except for special cases where Gaussian $(\alpha = 2)$, Cauchy $(\alpha = 1, \beta = 0)$ and Levy $(\alpha = 1/2\,, \beta = 1)$ distributions in (4.3) , the stable distribution can be generally characterized by its characteristic function $\varphi(\theta)$ given by (4.3) (Arce, 2005)

$$\varphi(\theta; \alpha, \beta, \sigma, \mu) = \exp[i\theta\mu + \sigma^{\alpha}(i\theta\omega(t; \alpha, \beta) - |\theta|^{\alpha})] \tag{4.3}$$

where the function $\omega(\theta; \alpha, \beta)$ is defined as (4.4).

$$\omega(\theta; \alpha, \beta) = \begin{cases} \beta|\theta|^{\alpha-1}\tan\frac{\pi\alpha}{2} & , \quad \alpha \neq 1 \\ -\beta\frac{2}{\pi}\log|\theta| & , \quad \alpha = 1 \end{cases} \tag{4.4}$$

The parameters characteristic exponent $\alpha \in (0, 2]$, skewness parameter $\beta \in [-1,1]$, scale parameter $\sigma > 0$ and the location parameter $-\infty < \mu < \infty$, tune the impulsiveness, symmetry, intensity and location of the distribution, respectively. The distribution is said to be symmetric for $\beta = 0$. The effect of skewness on probability density function (pdf) is illustrated in Figure 4.1a. The tail probabilities shown in Figure 4.1b indicate the effect of impulsiveness on pdf. The more impulsive noise (i.e. less characteristic exponent) results in the tails of the pdf to be heavier, that is why these distributions are also called as heavy tail distribution.

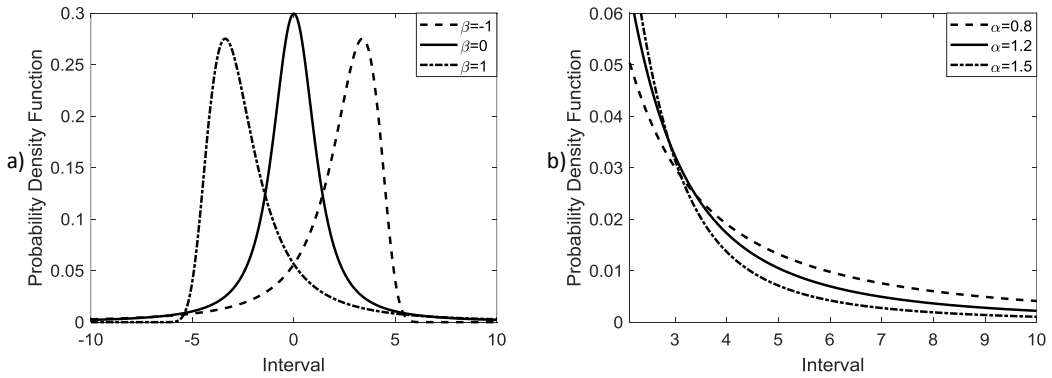

Figure 4.1 Illustration of probability density function of α −stable distribution for several parameters a) $\alpha = 1.2,\ \sigma = 1,\ \mu = 0$, b) Tail density $(\beta = 0,\ \sigma = 1,\ \mu = 0)$

One of the most significant properties of α −stable distribution is that only the fractional moments lower than α are finite. It can be expressed in terms of a stable random variable X as

$$\begin{matrix} E|X|^p < \infty & , & p < \alpha \\ E|X|^p = \infty & , & p \geq \alpha \end{matrix}. \tag{4.5}$$

According to the property given by (4.5) the variance is finite only for Gaussian noise where $\alpha = 2$. Correspondingly the variance of the distribution is infinite for $0 < \alpha < 2$. On the other hand, the mean value is finite only for $1 < \alpha \leq 2$ (Samorodnitsky & Taqqu, 1994). As a general property for $0 < \alpha < 2$, the p-th moment of the alpha-stable distribution is finite only for $0 < p < \alpha$. That is why this class of distribution is called as α −stable distribution. In the sequel, the mathematical description and the function of the robust estimators in observed data is explained.

4.2 Robust Estimators

Major aim of utilizing robust estimators is to filter the outlier components from the noisy observations. Since α −stable distributed noise inherently includes impulsive components depending on its characteristic exponent, there exists significant outliers which directly degrades the estimation accuracy of the PRI parameters. Basically,

there are three different methods called as median, myriad and meridian, explained respectively in the following subsections. These filters are commonly referred as maximum-likelihood estimators (or M-estimators) developed within the theory of robust statistics (Huber, 1981, Kassam & Poor, 1985). It is reported to use robust estimators crucial for impulsive signal processing, especially for which the noises are modelled by heavy-tailed distributions (Ilow, 1995; Nikias & Shao, 1995; Arce, 2005). The observed PRI-modulated signal $x[\cdot]$ under additive α −stable noise is modelled as

$$x[n] = s[n] + w[n] \qquad n = 1, \cdots, N \tag{4.6}$$

where $s[\cdot]$ is the noise free PRI-modulated signal including rectangular pulses with amplitude A, apart from each other in time axis according to the given PRI type. The noise samples $w[\cdot]$ are taken from the density represented in terms of its symmetric α −stable $(S\alpha S)$ noise parameters $w[\cdot] \sim S(\alpha, \beta = 0, \sigma, \mu = 0)$. Since the noise variance is known to be infinite for $\alpha < 2$, the metric for signal to noise ratio is redefined as generalized signal to noise ratio $(GSNR)$

$$GSNR = 10 \log \frac{A^2}{\sigma^\alpha} \tag{4.7}$$

Noting that the instant detection of pulses constitutes the main motivation of this thesis, differing from the conventional approach, the robust estimators are modified to process only past values of observations with respect to selected window length M. The mathematical formulization is given at the next subsections.

4.2.1 Median Filter

The filter output $y_{med}[n]$ given by (4.8) of a Median filter at time instant n observed from noisy measurements $x[n]$ is expressed as determining the median value between the samples of an observation interval having an even length of M arranged in ascending or descending order.

$$y_{med}[n] = \text{MEDIAN}\,(x[n-\text{M}], \ldots, x[n]) \tag{4.8}$$

4.2.2 Myriad Filter

Myriad estimator, comprehensively described in (Kalluri & Arce, 2000; Kalluri & Arce, 2001) is expressed as one of the robust estimators and the myriad estimator output $y_{myr}[n]$ at time instant n from noisy observations $x[n]$ is given by (4.9).

$$\begin{aligned} y_{myr}[n] &= \text{MYRIAD}\,(K;\ x[n-M], \ldots, x[n]). \\ &= \arg\min_{\rho \in \Re} \textstyle\sum_{i=n-M}^{n} \log[K^2 + (x[i]-\rho)^2] \end{aligned} \tag{4.9}$$

where the linearity parameter K is recommended to choose as a function of α $K = \sqrt{\frac{\alpha}{2-\alpha}}$ under α −stable noise (Arce, 2005). The selection of K strongly large (approximating to asymptotic limit $K \to \infty$), the myrad filter turns into the simple mean filter (Stork, 2010), and thus, would be in efficient in filtering the heavy-tailed noises. On the other hand, selection of K as small value (approximating to $K \to 0$) the estimator leads to multiple local minima, and thus, cannot estimate the location properly. Therefore, a predefined value for the linearity parameter K is significant for the optimal filtering result.

4.2.3 Meridian Filter

Similar to myriad filter, meridian filter has an approximate identical structure except the function expressing deviation from the actual value of the filter output. The meridian filter output $y_{mer}[n]$ at time instant n from noisy observations $x[n]$ as given (4.10):

$$\begin{aligned} y_{mer}[n] &= \text{MERIDIAN}\,(\Delta;\ x[n-M], \ldots, x[n]) \\ &= \arg\min_{\eta \in \Re} \textstyle\sum_{\text{i}=n-M}^{n} \log\,[\Delta + |x[i]-\eta|]. \end{aligned} \tag{4.10}$$

where Δ is the medianity parameter, and the even number M is length of the filter. In the case of the high values of Δ the filter behaviour converges to median filter for low values mode (Aysal & Kenneth, 2007).

The performance of these filters is analysed in terms of different filter length or different noise impulsiveness. Figure 4.2 illustrates the filtering performance in time domain. Although one can see that all off the filters provide a certain signal denoising, there is a time delay between the exact and estimated time instants on pulse onset.

a)

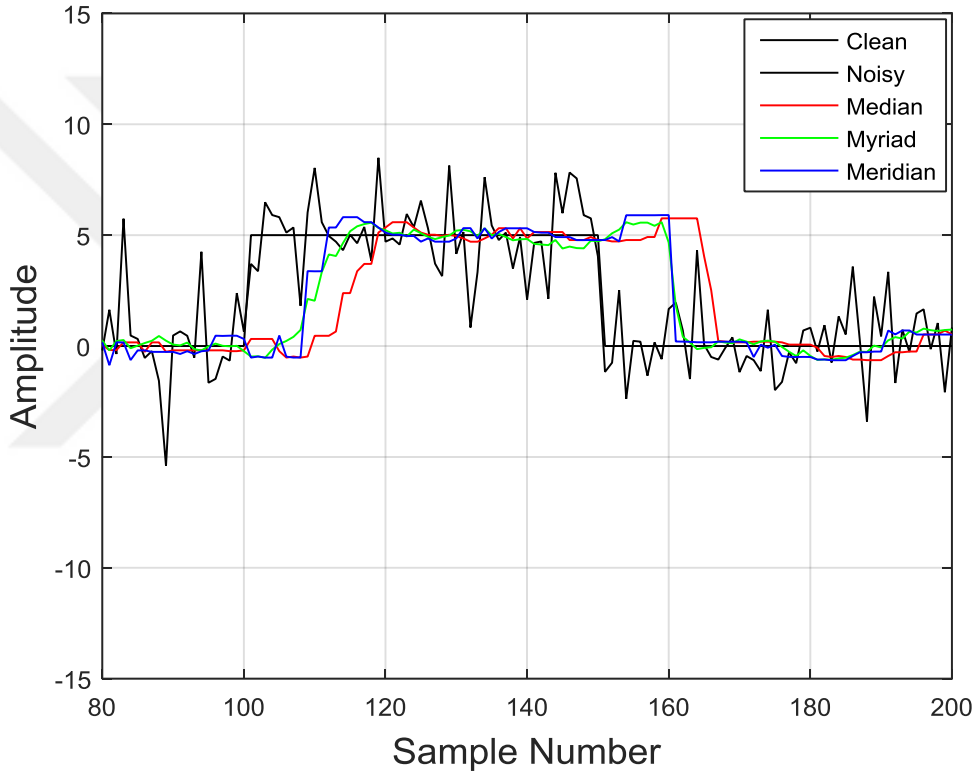

Figure 4.2 Time domain analysis of the robust estimators for a small segment of constant PRI data, ($\alpha = 1.5,\ M = 5$), $GSNR = 14\ dB$ (a) typical appearance, (b) zoomed in

b)

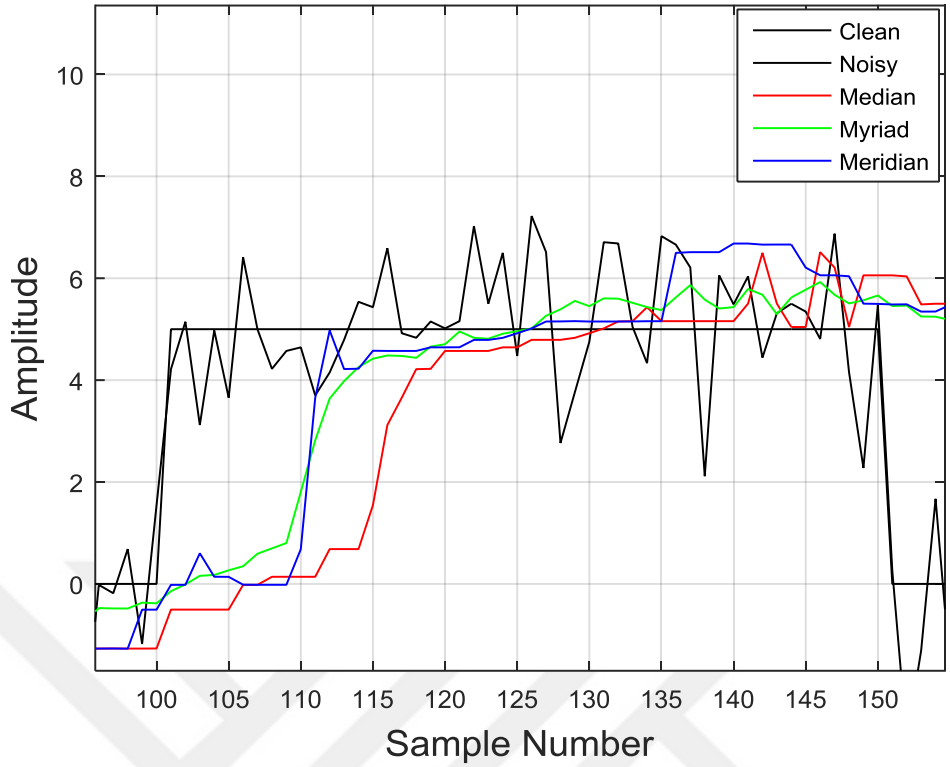

Figure 4.2 continues

Since the window function length M is relatively small, insufficient amount of data is used to filter the noisy signal the filter output is observed to have a notable deviation from exact data. In order to reduce this deviation which may cause to observe spurious or missed pulses, the robust filter outputs obtained by increasing filter length is shown in Figure 4.3. It is seen that increasing filter length ensures to prevent deciding spurious and/or missing pulses since the increased amount of data is processed the deviation from exact values decreases. However, the time delay to estimate pulse onset dramatically increases which degrades the detection performance. This result indicates that there is a trade-off between selection of filter length and the time delay from exact starting points of the pulses.

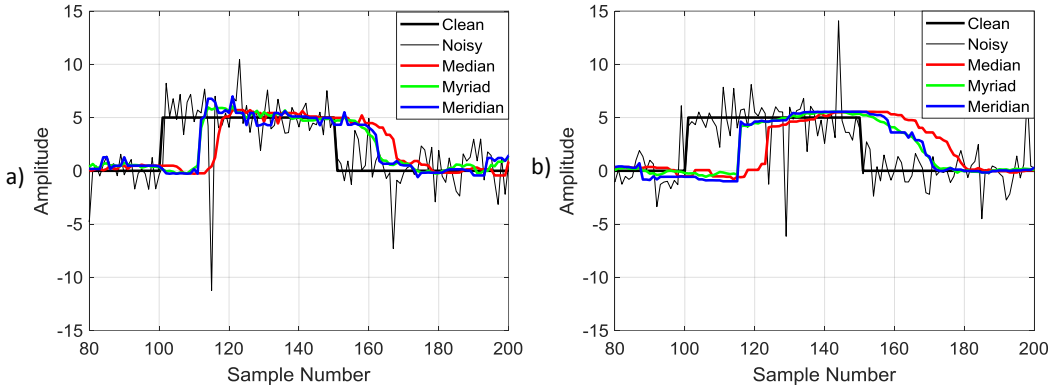

Figure 4.3 The effect of window length M on PRI data under α −stable noise, ($\alpha = 1.5$), $GSNR = 14\ dB$ a) $M = 11$, b) $M = 17$

The effect of impulsiveness of the noise is analysed in Figure 4.4a and Figure 4.4b. Since the impulsiveness of the noise decreases as the characteristic exponent α increases, the ripples in filtered data is observed to weaken. On the other hand, there is no apparent difference between time delays between actual pulse onset for both noise contamination. It can be said that noise impulsiveness can only an effect on occurring spurious or missing pulses.

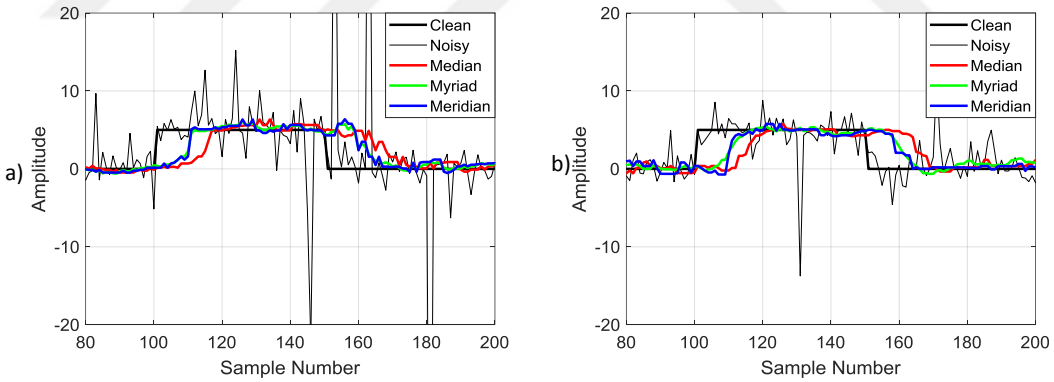

Figure 4.4 The effect of impulsiveness of the noise on PRI data under α −stable noise, $GSNR = 14\ dB$, $M = 11$, a) $\alpha = 1.3$, b) $\alpha = 1.7$

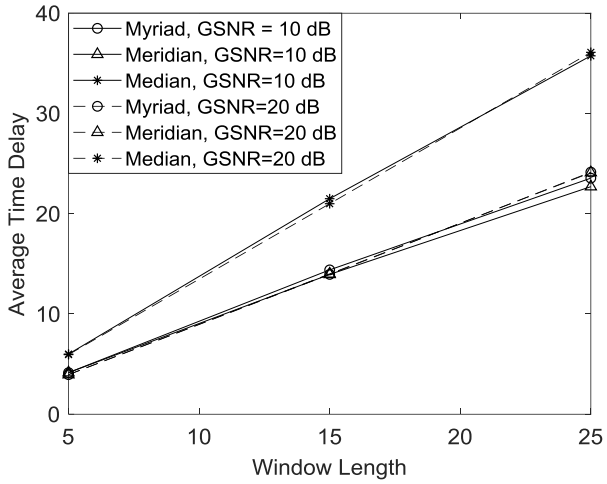

Figure 4.5 Average time delay of constant PRI-modulated data after robust filtering, $\alpha = 1.5$

Performance is analysed in terms of average time delay representing decision time after a particular pulse onset occurred shown by Figure 4.5. Simulations are evaluated on constant PRI waveform including two rectangular pulses having a length of 500 samples and ensemble averaging of 10 independent realizations. It can be clearly said that, the increasing window length strongly increases amount of delay of the detection timing, i.e. poor performance. On the other hand, due to robustness aspect against outlier components in non-Gaussian noise, the robust estimator performance does not apparently affect by variation of $GSNR$. Note that the characteristic exponent of the noise which tunes impulsiveness, does not directly affect the amount of delay. However, it is the reason of observing spurious pulses, and therefore an important parameter should be taken into account in PRI analysis under $\alpha-$stable noise environment.

4.3 Quickest Detection

In most of the signal processing applications, instant detection of abrupt changes has a vital importance. Basically, the quickest detection method determines the timing of instant variation as quick as possible depending on the selection of threshold. According to this method, two hypotheses represent the existence or absence of a signal within a certain time interval. Therefore, the two different states related with signal and noise probability density function are assumed to be known in advance.

Noting this assumption, cumulative summation (CUSUM) algorithm given comprehensively by (Page, 1954) is applied on observed data. In PRI recognition problem under noise, major aim is to find the time t_c corresponding to finding the time-of-arrivals (rising edges) of incoming rectangular radar pulses, so that the PRI pattern can be estimated.

In this problem, the CUSUM algorithm assumes two hypotheses $\mathcal{H}_0$ and $\mathcal{H}_1$ under the prescribed probability distribution function (PDF) of the noise in the channel. $\mathcal{H}_0$ assumes the observed signal contains only the noise, and $\mathcal{H}_1$ assumes an existence of a constant deterministic signal of amplitude A together with noise. Differing from off line data analysis which formulates the problem considering time of arrival, the problem is mathematically expressed as existence or absence of an incoming signal according to the observation given by the two hypotheses above. The binary hypotheses testing problem given by (4.11) includes varian of parameter Θ

$$\begin{matrix} \mathcal{H}_0: & \Theta = \Theta_0 & \text{for } 1 \leq i \leq k \\ \mathcal{H}_1: & \Theta = \Theta_1 & \text{for } 1 \leq i \leq k \end{matrix} \quad , \tag{4.11}$$

where Θ is a conditional density parameter and $\Theta_0 = 0$ corresponding only noise and $\Theta_1 = A$ for existence of constant signal and noise. These hypotheses compose the likelihoods formulated by probability density function of the channel noise represented by $f_0(x)$ and $f_1(x)$, respectively. The log-likelihood ratio including observation from the beginning until the end of the observation point k is defined as (Basseville & Nikiforov, 1993)

$$S_k = \sum_{i=1}^{k} \ln \frac{f_1(x[i])}{f_0(x[i])} \tag{4.12}$$

which constitutes the skeleton of the cumulative summation (CUSUM). That is why this method is also named as CUSUM method. Principally, the CUSUM algorithm utilizes the information obtained from instantaneous log-likelihood ratio $\ln \frac{f_1(x[i])}{f_0(x[i])}$ and detects the deviation within an observation interval having length k. In the time-varying CUSUM approach, this observation interval is designed to slide when new

data point is observed and the statistics is derived from the new data having the same length. According to provide the same analogy, it can be accepted as $k = M$. Considering step by step, when $f_0(x[i]) > f_1(x[i])$, the ratio is less than unity, and thus, the logarithm is negative. Under the cumulative summation, the log-likelihood S_k decreases for increasing k, provided that the incoming signal is just a noise (hypothesis $\mathcal{H}_0$). When observation includes data from deterministic signal, the hypothesis $\mathcal{H}_1$ becomes valid, i.e. $f_0(x[i]) < f_1(x[i])$. This gives $\frac{f_1(x[i])}{f_0(x[i])} > 1$, and hence $\ln\frac{f_1(x[i])}{f_0(x[i])} > 0$. Therefore, under the cumulative summation, the log-likelihood S_k begins to increase with increasing k. One can detect the change between decresing and increasing S_k to determine the time-of-arrival θ by defining a threshold h. For this purpose, it is defined by (4.12) that a decision function (Basseville & Nikiforov, 1993).

$$G_k = S_k - \min_{1 \le j \le k} S_j. \tag{4.12}$$

The decision function lies in certain different ranges according to the absence or existence of the deterministic signal, constant pulse having amplitude A, as in this application. Variation of the decision function G_k is compared with a predefined threshold h, to determine the rising edge time θ. Under the absence of pulse, $G_k < h$. The estimated time-of-arrival is accepted to be the first time instant when decision function becomes larger than the threshold, i.e., $G_\theta > h$. By tuning this threshold, the false alarms rate can be arranged, where the false alarm causes the rises in the decision function due to impulsive nature of the channel noise. Figure 4.6a illustrates noise free constant PRI data and Figure 4.6b represents the variation of function G_k analysed within sliding time window k under $S\alpha S$ noise with $\alpha = 1.5$ and $GSNR = 14\ dB$. It is seen that an abrupt change at starting point of pulses can be detected using only present point k and past points up to $k - M$ corresponding to the initial point of the sliding window.

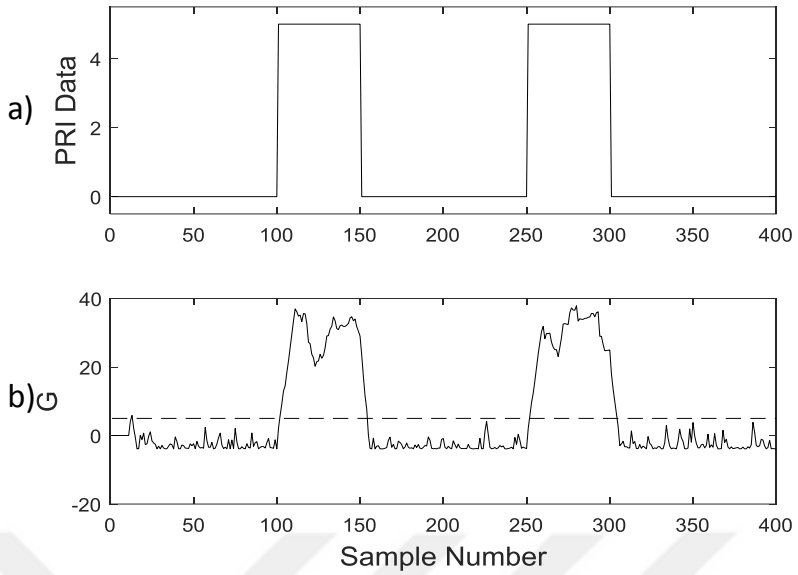

Figure 4.6 a) Noise free PRI waveform, b) Decision function $G(k)$. $A = 5, M = 11, h = A$

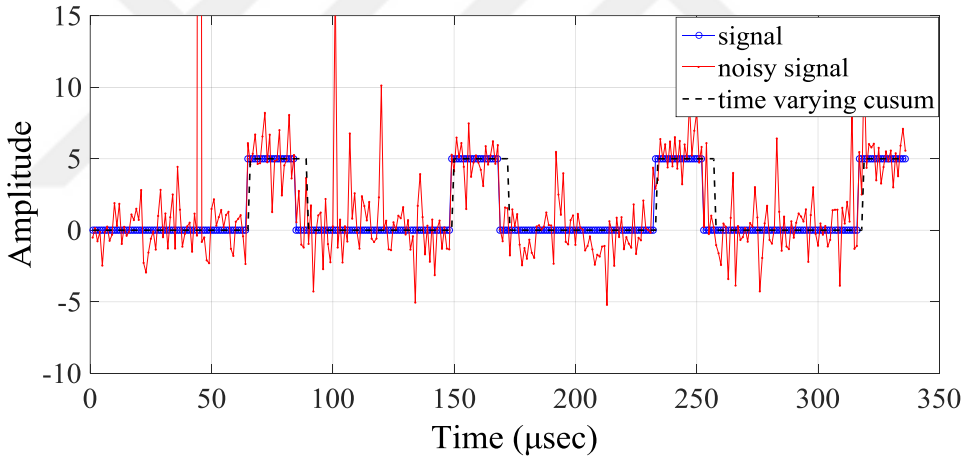

Figure 4.7 Time varying CUSUM based quickest detected signals for Constant PRI modulated signal

The exact PRI data, noisy and detected PRI data are shown together in Figure 4.7 It is quite apparent that the CUSUM method yields instant detection of rising edges of rectangular pulses compared with the robust estimators which do not use pdf of the data and estimates rising edge times only from the observations. This can be one of the reasons of CUSUM based quickest method to be more superior than robust estimators.

CHAPTER FIVE
CONCLUSION

In this thesis study, characterizing and detecting time of arrival of PRI modulated signals are analysed. The first part of the thesis is based on describing three features generated from correlation and power spectral density, like the methods given in the literature. It is remarked that the different PRI pattern can be characterized and classified by using basic signal processing tools to extract statistical behaviour of different PRI patterns.

However, in radar signal processing related with PRI-modulated signals the contaminated noise generally assumed to be Gaussian and the effect of its intensity is not investigated in details. The main contribution of the thesis is the detection of PRI-modulated signals under non-Gaussian noise environment. The proper and reasonable selection for non-Gaussian noise is α −stable distributions. Once the time of arrival of the rectangular radar pulses are determined by providing minimum time delay than its actual value, the PRI patterns can be characterized easily.

As the first approach, robust M-estimators such as median, myriad and meridian filters are utilized to filter impulsive noise. Since the main requirement is instant detection of incoming radar pulse, differing from the literature, all of these robust estimator designs are modified to use only present and past values whose length is determined by window size. It is observed that the increasing window length provides stronger filtering performance which is significant to avoid spurious pulses when the noise impulsiveness is notable. However, on the other hand, the detection of time of arrival of rectangular pulse has an increased time delay which is not required. One can say that there is a trade-off between selection of window length and estimation delay. when the performances of robust estimators are compared with each other when the GSNR and window lengths are kept to be fixed, one can see that myriad and meridian filters yields better performance than median filter which is simplest to implement.

In order to provide an instant detection of rising edges of the rectangular pulses, to the best of our knowledge, quickest detection algorithm is applied for the first time in the literature. The CUSUM algorithm is redefined to propose a time-varying nature so that a time-varying CUSUM algorithm determines the time onset of the radar pulses depending on the pre-defined threshold value. It is shown that time-varying CUSUM based quickest detection method provides superior performance compared with robust estimators. As key note, it should be taken into account that the quickest detection method needs probability density function of the contaminated noise in order to provide likelihood ratio test. Both robust estimator and quickest detection methods assume the pulse amplitude is known in advance to tune the threshold and constructing likelihood function, respectively.

The main challenge on quickest detection method is to tune the threshold value which directly related with false alarm rate. Differing from the conventional receiver operating characterization, the threshold varies with respect to observed data and an adaptive method is needed to describe the performance of the proposed method in terms of false alarm probability. This constitutes the future projections of this research.

REFERENCES

Ahmadi, M., & Mohamedpour, K. (2012). PRl modulation type recognition using level clustering and autocorrelation. *American Journal of Signal Processing, 2* (5), 83-91.

Arce, G. R., (2005*). Nonlinear Signal Processing*, New Jersey, USA: J. Wiley & Sons.

Avionics Department. (2013). *Electronic Warfare and Radar System Engineering Handbook* (4th ed.). California: Technical Communication Office.

Aysal, C. T., & Kenneth, E. B. (2007). Robust meridian filtering. *Proceedings of International Conferences on Acoustic, Speech and Signal Processing, 3,* 741-744.

Basseville, M., & Nikiforov I.V. (1993). *Detection of Abrupt Changes: Theory and Application*. Englewood Cliffs: Prentice-Hall.

Broersen, P.M.T. (2006). *Automatic Autocorrelation and Spectral Analysis.* Netherlands:Springer.

Conroy, T., & Moore, J.B. (1998). The limits of extended Kalman Filtering for pulse train deinterleaving. *IEEE Transactions on Signal Processing, 46* (12), 3326 – 3332.

Conroy, T., & Moore J.B. (2000). On the estimation of interleaved pulse train phases. *IEEE Transactions on Signal Processing, 48* (12), 3420-3425.

Davies, C.L. & Hollands, P. (1982). Automatic processing for ESM. *IEE Proceedings F (Communications, Radar and Signal Processing), 129*, 164-171.

Ghani, K. A., & Dimyati, K., & Sha'ameri, A. Z., & Daud, N. G. N. (2016). Statistical modeling for missing and spurious pulses in pulse repetition interval (PRI) Analysis. *Defence S&T Technical Bulletin, 9,* 18-27.

Ghani, K. A., & Sha'ameri, A. Z., & Dimyati, K., & Daud, N. G. (2017). Pulse repetition interval analysis using decimated Walsh-Hadamard Transform. *2017 IEEE Radar Conference,* 58-63.

Gençol, K., & At, N., & Kara, A. (2016). A wavelet-based feature set for recognizing interval modulation patterns. *Turkish Journal Of Electrical Engineering & Computer Sciences*, *24*, 3078-3090.

Giles, L. (1910). *Sun Tzu On The Art of War*. London: Luzac and Company.

Huber, P. J. (1981). *Robust statistics.* New York: Wiley.

Hu, G., & Liu Y. (2010). An efficient method of pulse repetition interval modulation recognition. *International Conference on Communications and Mobile Computing*, *2*, 287-291.

Ilow, J. (1995). *Signal processing in alpha-stable noise environments: noise modeling, detection and estimation*. Phd Thesis, University of Toronto, Canada.

Joint Chiefs of Staff. (2012). *Joint Electromagnetic Spectrum Management Operations.* United States: Joint Chiefs of Staff.

Kalluri, S., & Arce, G. R. (2000). Fast algorithms for weighted myriad computation by fixed point search. *IEEE Transactions on Signal Processing, 48,* 159–171.

Kalluri, S., & Arce, G. R. (2001). Robust frequency-selective filtering using weighted myriad filters admitting real-valued weights. *IEEE Transactions on Signal Processing, 49* (11), 2721–2733.

Kassam, S. A., & Poor, H. V. (1985). Robust techniques for signal processing, *Proceedings of the IEEE, 73* (3), 433-481.

Kauppi, J. P., & Martikainen, K. S. (2007). An efficient set of features for pulse repetition interval modulation recognition. *2007 IET International Conference on Radar Systems.* 1-5.

Katsilieris, F., & Apfeld S., & Charlish A. (2017). Correlation based classification of complex PRI modulation types. *2017 Sensor Signal Processing for Defence Conference (SSPD): London , UK*, 25-29.

Kuang, Y., & Shi, Q. (2005). A simple way to deinterleave repetitive pulse sequences. *7th WSEAS International Conference on Mathematical Methods and Computational Techniques in Electrical En*gineering: Sofia, 218-222,

Kumar U., & Dhananjayulu.V,, & Kumar.A. (2014). Deinterleaving of radar signals and its parameter estimation in EW environment. *International Journal of Emerging Technology and Advanced Engineering, 4* (9),490-494.

Liu Y., & Zhang, Q. (2017). An improved algorithm for PRI modulation recognition. *2017 IEEE International Conference on Signal Processing, Communications and Computing (ICSPCC),* 1-5.

Logothetis, A., & Krishnamurthy, V. (1998). An interval-amplitude algorithm for deinterleaving stochastic pulse train sources. *IEEET Signal Processing, 46,* 1344-1350.

Mahdavi, A. & Pezeshk, A. M. (2010). A robust method for PRI modulation recognation. *IEEE International Conference on Signal Processing (ICSP),* 1873-1876.

Mardia, H.K. (1989). New techniques for the deinterleaving of repetitive sequences. *IEE Proceedings F - Radar and Signal Processing, 136*, 149-154.

Milojevic, D.J., & Popovic, BM. (1992). Improved algorithm for deinterleaving of radar pulses. *IEE Proceedings F - Radar and Signal Processing, 139* (1), 98-104.

Moore, J.B., & Krishnamurthy, V. (1994). Deinterleaving pulse trains using discrete-time stochastic dynamic-linear models. *IEEE T Signal Processing*; *42*, 3092-3103.

Nikias, C.L., & Shao, M. (1995). *Signal Processing with Alpha-Stable Distributions and Applications* (1th ed.). New York: Wiley-Interscience.

Nikiforov, I., & Basseville, M. (1993). *Detection of Abrupt Changes: Theory and Application*. New Jersey: Prentice-Hall, Inc.

Noone, G.P. (1999). A neural approach to tracking radar pulse repetition interval modulations. *Neural Networks for Signal Processing IEEE, 3*, 1075-1080.

Noone, G.P. (1999). A neural approach to automatic pulse repetition interval modulation recognition. *1999 Signal Processing and Communications Symposium,* 213-218.

Orsi, R.J., & Moore, JB., & Mahony RE. (1999). Spectrum estimation of interleaved pulse trains. *IEEET Signal Processing, 47*, 1646-1653.

Poise, R.A. (2013). *Information Warfare and Electronic Warfare Systems*. Boston, London: Artech House.

Ryoo, Y.J., & Song, K.H., & Kim, W.W. (2007). Recognition of PRI modulation types of radar signals using the autocorrelation. *Institute of Electronics, Information and Communication Engineers, 90*, 1290–1294.

Samorodnitsky, G., & Taqqu, M. S. (1994). *Stable Non-Gaussian Random Processes*. London: Chapman and Hall/CRC.

Shi, Z., & Wu, H., & Shen, W., & Cheng, S., & Chen Y. (2016). Feature extraction for complicated radar PRI modulation modes based on auto-correlation function. *IEEE Advanced Information Management, Communicates, Electronic and Automation Control Conference (IMCEC)*, 1617-1620.

Skolnik, M. I. (1990). *Radar Handbook.* (2nd ed.). Boston: McGraw-Hill.

Skolnik, M. I. (1981). *Introductıon to Radar Handbook*. (3nd ed.). Singapore: McGraw-Hill.

Stoica, P., & Moses, R. (2005). *Spectral Analysis of Signals.* New Jersey: Prentice Hall.

Stork, M. (2010). Adaptive weighted meridian nonlinear filter used for filtering of signal with impulsive noise. *Proceedings of the International Conference on Circuits, Systems, Signals*, 359-364.

Page, E. S. (1954). Continuous inspection schemes, *Biometrika*, *41* (1-2), 100–115.

Wiley, R. (2006). *ELINT*: *The Interception and Analysis of Radar Signals.* Massachusetts: Artech House.